Electronic Supplementary Material (ESI) for Dalton Transactions.

Supporting Information for

Tuning the stability of bimetallic Ce(IV)/Zr(IV)- based MOFs with UiO-66 and MOF-808 structure

Martin Lammert, Christian Glißmann and Norbert Stock

2. Characterization of Ce/Zr-UiO-66

3. Characterization of Ce/Zr-MOF-808

1. Synthesis procedures

Materials and Methods. Cerium ammonium nitrate (98 %, $(NH_4)_2Ce(NO_3)_6$, Alfa Aesar), 1,4-benzenedicarboxyic acid (98 %, H_2BDC, Sigma Aldrich), benzene-1,3,5-tricarboxylic acid (95 %, H_3BTC, Sigma Aldrich), zirconium(IV) dinitrate oxide hydrate ($ZrO(NO_3)_2 \cdot H_2O$, ABCR), zirconium(IV) chloride (99 %, $ZrCl_4$, Sigma Aldrich) were used as obtained.

PXRD characterization for product identification was performed on a STOE Stadi P Combi diffractometer with $MoK_{\alpha 1}$ radiation or with $CuK_{\alpha 1}$ radiation, equipped with a Mythen 1K detector system and a xy-stage. The high resolution PXRD patterns were recorded on a Stadi P diffractometer with $CuK_{\alpha 1}$ radiation using a Mythen 1K detector. Therefore samples were prepared by mixing the Ce/Zr-MOFs with potassium chloride (approximately molar ratio 6:1) acting as internal standard reagent, respectively and thoroughly grinded before PXRD data were collected. The lattice parameters of the bimetallic MOFs were calculated using the Le Bail method implemented in the program TOPAS Academic v4.1. Simultaneously the structure of KCl (a= 6.2890(2) Å) was refined by Rietveld methods using the same program, with the result to minimize errors e.g. zero point shift, during the determination.

For variable temperature X-ray diffraction measurements, the STOE Stadi P Combi diffractometer with $MoK_{\alpha 1}$ radiation was equipped with a capillary furnace. These measurements were carried out under air in a 0.5 mm quartz capillary in a range of 1-19° 2θ with a measuring time of 3 min after each 5 °C temperature step. At the temperature were the crystallinity drastically decreases the thermal stability was specified. Due to the 5 °C temperature step an error of ±5 °C must be considered.

Sorption experiments were performed using a BEL Japan Inc. Belsorpmax. The specific surface areas were determined using the Rouquerol[1] approach and the micropore volume was calculated at $p/p_0 = 0.5$. Thermogravimetric measurements were performed on a TA instruments Q500 under air flow (10 ml min^{-1}) with a heating rate of 4 K min^{-1}. Energy-dispersive X-ray (EDX) spectroscopy data were recorded on a Philips XL30 FEG microscope. Each sample was measured three times at different spots. From the data the average values in at% of Ce, Zr and the standard deviation were calculated. The particle sizes were measured using a Beckman Coulter Delsa™ Nano C Particle Analyzer. Therefore prior to measurement the samples were dispersed in ethanol for 30 min in an ultrasonic bath.

Synthesis of Ce/Zr-UiO-66. Mixed Ce/Zr-UiO-66 solid solutions were synthesized using Pyrex glass reaction tubes (V_{max}= 14 mL). 1,4-benzendicarboxylic acid (H_2BDC, 127.6 mg) was introduced into the glass reactor and N,N-dimethylformamide (DMF, 3.6 mL) and aqueous solutions of cerium(IV) ammonium nitrate (0.533 M), zirconium(IV) dinitrate oxide hydrate (0.533 M) and concentrated formic acid (HCOOH, 100 %, 1.03 mL) were added. The starting conditions are identical for all syntheses. The variation of the Ce/Zr ratio is possible by varying the molar ratio of the starting materials (Tab. S1).

Tab. S1. Conditions for the synthesis of solid solutions of Ce/Zr-UiO-66.

Sample	**Ratio**				**Ce [µL]**	**Zr [µL]**	**H_2BDC [mg]**	**HCOOH [mL]**	**DMF [mL]**
	Ce	Zr	H_2BDC	HCOOH					
P1	0.5	5.5	7.2	256	100	1100	127.6	1.03	3.6
P2	1.0	5.0	7.2	256	200	1000	127.6	1.03	3.6
P3	1.5	4.5	7.2	256	300	900	127.6	1.03	3.6
P4	2.0	4.0	7.2	256	400	800	127.6	1.03	3.6
P5	2.5	3.5	7.2	256	500	700	127.6	1.03	3.6
P6	3.0	3.0	7.2	256	600	600	127.6	1.03	3.6
P7	3.5	2.5	7.2	256	700	500	127.6	1.03	3.6
P8	4.0	2.0	7.2	256	800	400	127.6	1.03	3.6
P9	4.5	1.5	7.2	256	900	300	127.6	1.03	3.6
P10	5.0	1.0	7.2	256	1000	200	127.6	1.03	3.6
P11	5.5	0.5	7.2	256	1100	100	127.6	1.03	3.6

After all starting materials were added the glass reactors were sealed and heated using an aluminum heating block under stirring for 15 min at 100 °C. The light yellow precipitate was centrifuged in the mother liquor, which was then decanted off, before being re-dispersed and centrifuged twice in DMF (2 mL). To remove DMF from the product, the solid was washed and centrifuged with acetone (2 mL) four times. The resulting white solid was dried in air at 70 °C.

Synthesis of Ce/Zr-MOF-808. Mixed Ce/Zr-MOF-808 solid solutions were synthesized using Pyrex glass reaction tubes (maximum volume 14 mL). 1,3,5-benzenetricarboxylic acid (H_3BTC, 67.2 mg), was introduced into the glass reactor and N,N-dimethylformamide (DMF, 1.6 mL) and aqueous solutions of cerium(IV) ammonium nitrate (0.533 M), zirconium(IV) dinitrate oxide hydrate (0.533 M) and concentrated formic acid (HCOOH, 100 %, 4.12 mL) were added. The starting conditions are identical for all syntheses. The variation of the Ce/Zr ratio is possible by varying the molar ratio of the starting materials (Tab. S2).

Tab. S2. Lattice parameters of the Ce/Zr-UiO-66 compounds obtained by Le Bail profile fitting.

Sample	**Ratio**				**Ce [µL]**	**Zr [µL]**	**H_2BTC [mg]**	**HCOOH [mL]**	**DMF [mL]**
	Ce	Zr	H_2BDC	HCOOH					
M1	1.0	5.0	3.0	1024	200	1000	67.2	4.12	1.6
M2	2.0	4.0	3.0	1024	400	800	67.2	4.12	1.6
M3	3.0	3.0	3.0	1024	600	600	67.2	4.12	1.6
M4	4.0	2.0	3.0	1024	800	400	67.2	4.12	1.6
M5	5.0	1.0	3.0	1024	1000	200	67.2	4.12	1.6

After all starting materials were added, the glass reactors were sealed and heated using an aluminum heater block under stirring for 20 min at 100 °C. The light yellow precipitate was centrifuged in the mother liquor, which was then decanted off, before being re-dispersed and centrifuged twice in DMF (2 mL). To remove DMF from the product, the solid was washed and centrifuged with acetone (2 mL) four times. The resulting white solid was dried in air at 70 °C.

Pure Ce-UiO-66 and Zr-UiO-66 were synthesized for comparison and according the synthesis method described in literature.[2,3]

2. Characterization of Ce/Zr-UiO-66

2.1. Results of the EDX analyses

Tab. S3: Results of the EDX analysis of the bimetallic Ce/Zr-UiO-66 compounds.

Sample	Elements	1. / at%	2. / at%	3. / at%	4. / at%	Mean value / at%	Standard deviation / at%
P1	Zr	91.94	92.86	90.13	91.88	91.7	1.1
	Ce	8.06	7.14	9.87	8.12	8.3	1.1
P2	Zr	84.13	85.42	84.53	84.15	84.6	0.6
	Ce	15.87	14.58	15.47	15.85	15.4	0.6
P3	Zr	82.71	82.01	81.22	82.38	82.1	0.6
	Ce	17.29	17.99	18.78	17.62	17.9	0.6
P4	Zr	79.76	78.74	80.23	78.85	79.4	0.7
	Ce	20.24	21.26	19.77	21.15	20.6	0.7
P5	Zr	77.92	78.05	76.85	77.41	77.6	0.5
	Ce	22.08	21.95	23.15	22.59	22.4	0.5
P6	Zr	72.69	74.72	73.61	73.06	73.5	0.9
	Ce	27.31	25.28	26.39	26.94	26.5	0.9
P7	Zr	65.56	65.35	65.7	67.11	65.9	0.8
	Ce	34.44	34.65	34.3	32.89	34.1	0.8
P8	Zr	60.00	59.05	58.56	59.61	59.3	0.6
	Ce	40.00	40.95	41.44	40.39	40.7	0.6
P9	Zr	49.88	49.11	48.67	49.83	49.4	0.6
	Ce	50.12	50.89	51.33	50.17	50.6	0.6
P10	Zr	33.73	34.37	34.59	34.91	34.4	0.5
	Ce	66.27	65.63	65.41	65.09	65.6	0.5
P11	Zr	20.22	21.85	22.49	19.77	21.1	1.3
	Ce	79.78	78.15	77.51	80.23	78.9	1.3

Fig. S4. Comparison of the molar ratio of Ce:Zr used for the synthesis of mixed-metal Ce/Zr-UiO-66 with composition [$Ce_xZr_yO_4(OH)_4(BDC)_6$] and measured by EDX analysis.

Sample	**Ce_x:Zr_y [at%] measured by EDX**	**Ce_x:Zr_y calculated from EDX**	**Ce_x:Zr_y used for synthesis**
P1	8.3 : 91.7	0.5 : 5.5	0.5 : 5.5
P2	15.4 : 84.6	0.9 : 5.1	1.0 : 5.0
P3	17.9 : 82.1	1.1 : 4.9	1.5 : 4.5
P4	20.6 : 79.5	1.2 : 4.8	2.0 : 4.0
P5	22.4 : 77.6	1.3 : 4.7	2.5 : 3.5
P6	26.5 : 73.5	1.6 : 4.4	3.0 3.0
P7	34.1 : 65.9	2.0 : 4.0	3.5 : 2.5
P8	40.7 : 59.3	2.4 : 3.6	4.0 : 2.0
P9	50.6 : 49.4	3.0 : 3.0	4.5 : 1.5
P10	65.6 : 34.4	3.9 : 2.1	5.0 : 1.0
P11	78.9 : 21.1	4.7 : 1.3	5.5 : 0.5

2.2. Powder X-ray diffraction

Tab. S5. Lattice parameters of all bimetallic UiO-66 compounds obtained by Le Bail profile fitting with KCl (a = 6.2890(2) Å) as internal standard.

Sample	**SG**	***a* [Å]**	**R_{wp} /%**	**GoF**
P1	$Fm\bar{3}m$	20.8028(8)	4.13	1.99
P2	$Fm\bar{3}m$	20.8636(7)	4.31	1.95
P3	$Fm\bar{3}m$	20.8714(6)	3.91	1.87
P4	$Fm\bar{3}m$	20.8988(4)	4.23	2.01
P5	$Fm\bar{3}m$	20.9198(4)	4.27	1.96
P6	$Fm\bar{3}m$	20.9469(5)	5.00	2.32
P7	$Fm\bar{3}m$	20.9867(4)	5.62	2.50
P8	$Fm\bar{3}m$	21.0329(3)	4.37	1.74
P9	$Fm\bar{3}m$	21.1022(3)	4.66	1.75
P10	$Fm\bar{3}m$	21.2282(4)	7.17	2.16
P11	$Fm\bar{3}m$	21.3511(3)	7.88	2.11

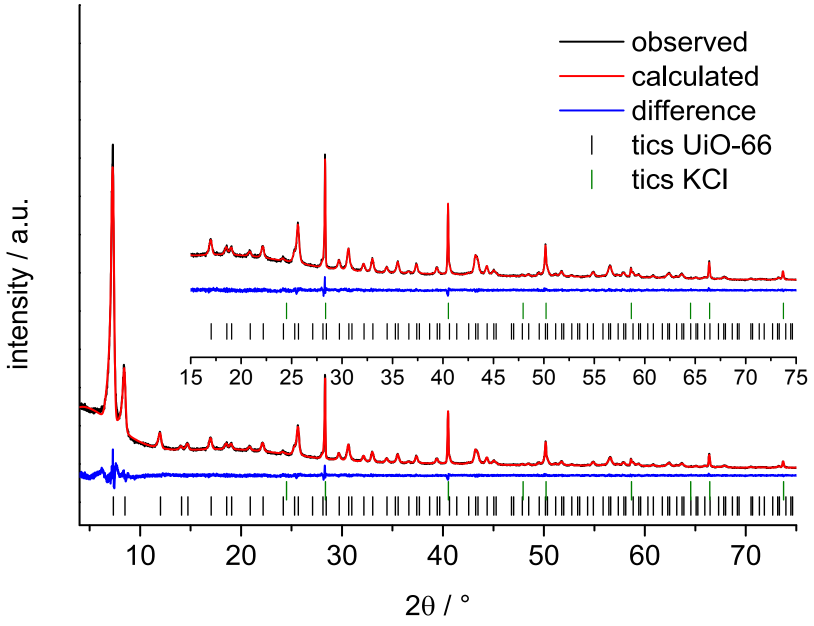

Fig. S1. Le Bail plot of UiO-66 sample P1. The observed PXRD pattern (λ= 1.5401 Å) is shown in black, the calculated in red and the difference (observed - calculated) of both patterns is given in blue. The allowed reflection positions of the peaks are given as black and green (KCl) tics.

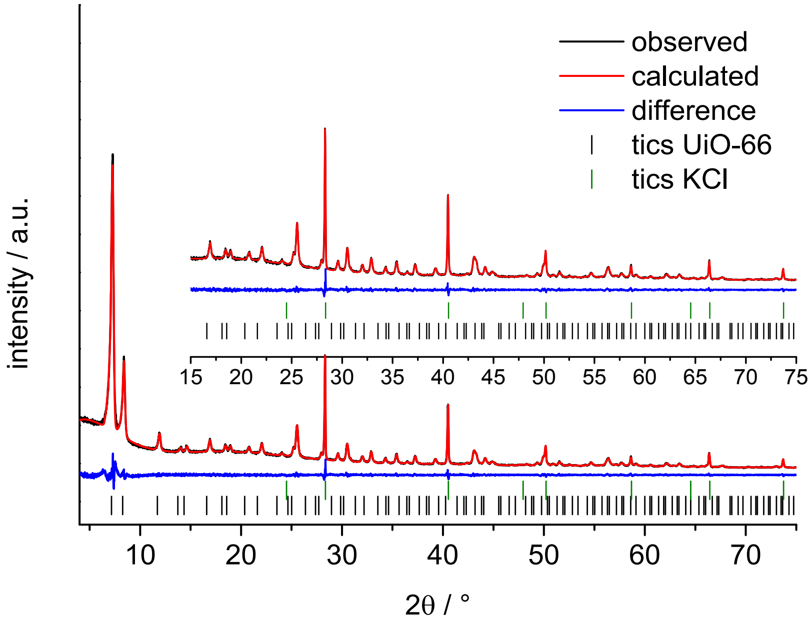

Fig. S2. Le Bail plot of UiO-66 sample P2. The observed PXRD pattern (λ= 1.5401 Å) is shown in black, the calculated in red and the difference (observed - calculated) of both patterns is given in blue. The allowed reflection positions of the peaks are given as black and green (KCl) tics.

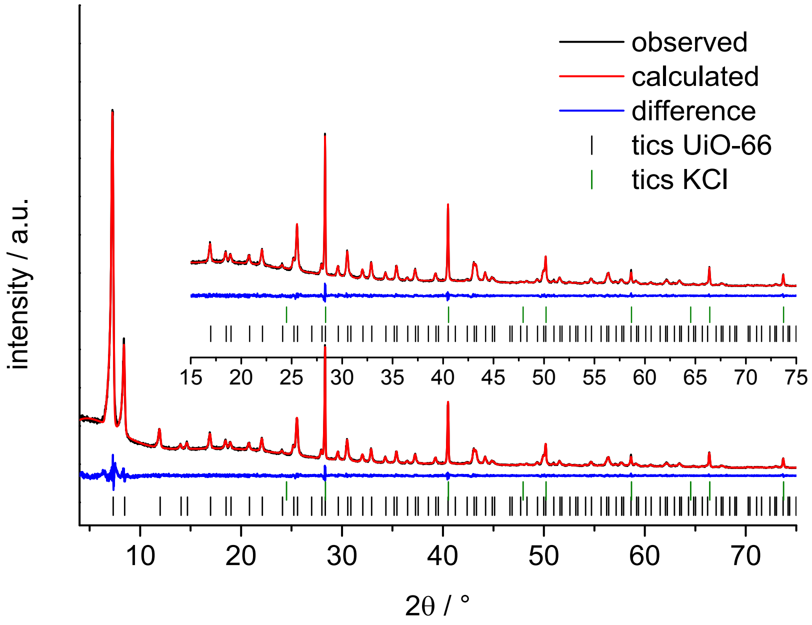

Fig. S3. Le Bail plot of UiO-66 sample P3. The observed PXRD pattern (λ= 1.5401 Å) is shown in black, the calculated in red and the difference (observed - calculated) of both patterns is given in blue. The allowed reflection positions of the peaks are given as black and green (KCl) tics.

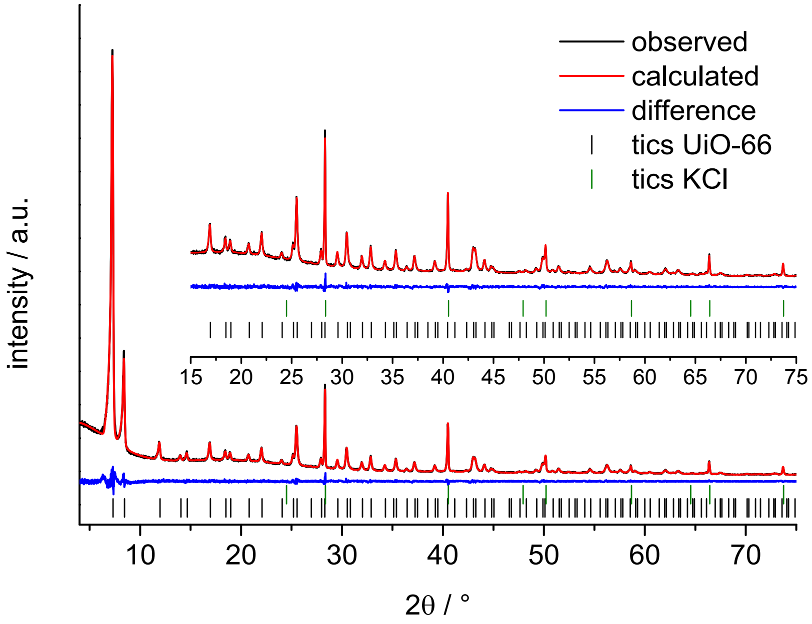

Fig. S4. Le Bail plot of UiO-66 sample P4. The observed PXRD pattern (λ= 1.5401 Å) is shown in black, the calculated in red and the difference (observed - calculated) of both patterns is given in blue. The allowed reflection positions of the peaks are given as black and green (KCl) tics.

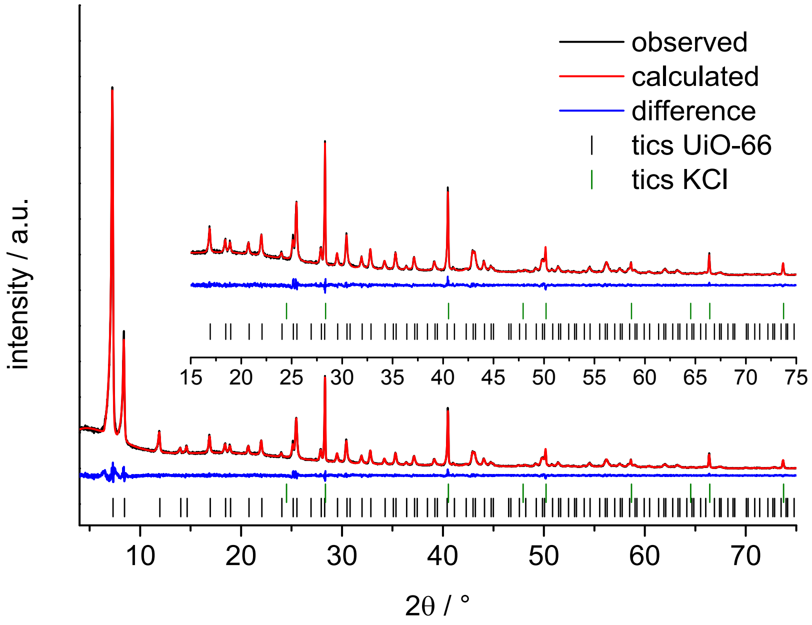

Fig. S5. Le Bail plot of UiO-66 sample P5. The observed PXRD pattern (λ= 1.5401 Å) is shown in black, the calculated in red and the difference (observed - calculated) of both patterns is given in blue. The allowed reflection positions of the peaks are given as black and green (KCl) tics.

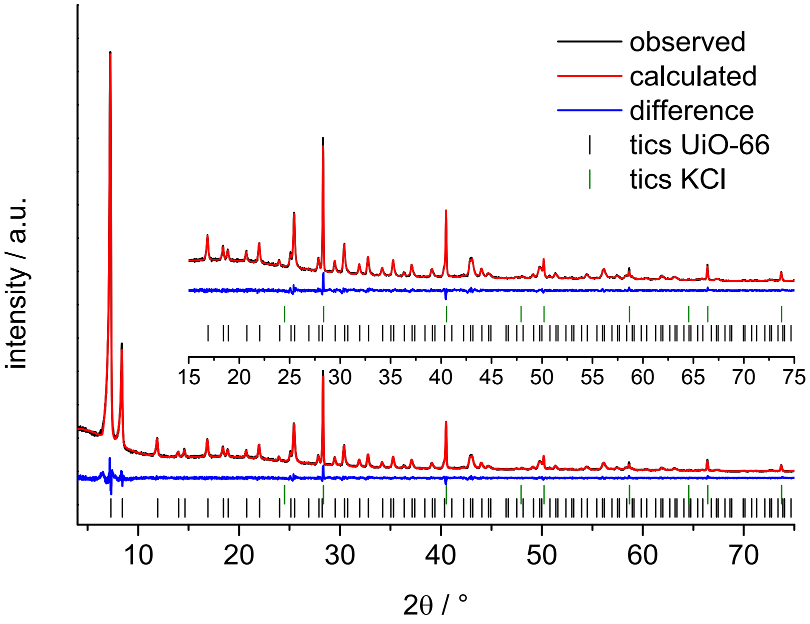

Fig. S6. Le Bail plot of UiO-66 sample P6. The observed PXRD pattern (λ= 1.5401 Å) is shown in black, the calculated in red and the difference (observed - calculated) of both patterns is given in blue. The allowed reflection positions of the peaks are given as black and green (KCl) tics.

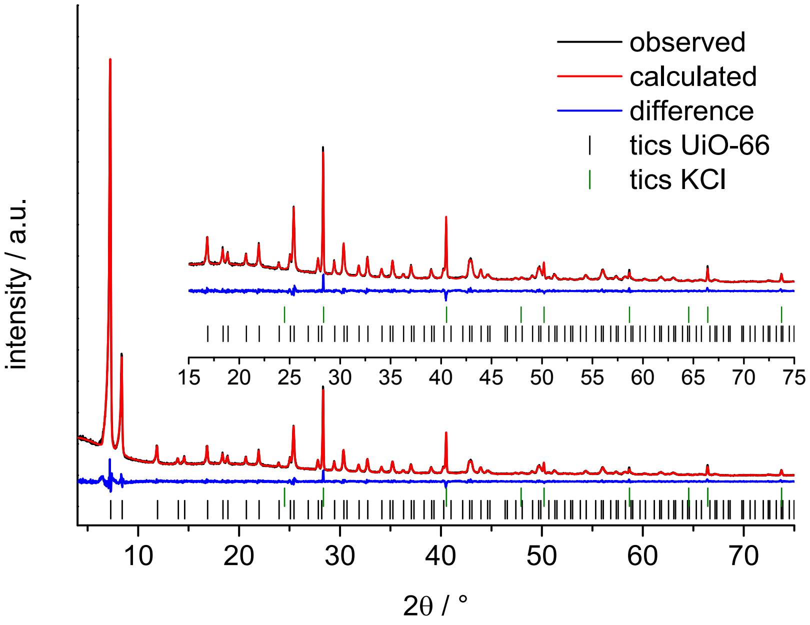

Fig. S7. Le Bail plot of UiO-66 sample P7. The observed PXRD pattern (λ= 1.5401 Å) is shown in black, the calculated in red and the difference (observed - calculated) of both patterns is given in blue. The allowed reflection positions of the peaks are given as black and green (KCl) tics.

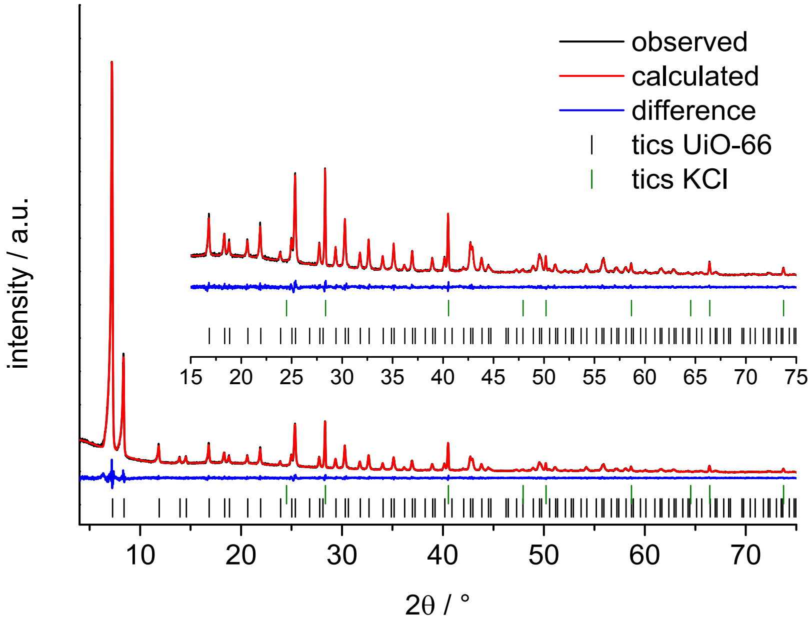

Fig. S8. Le Bail plot of UiO-66 sample P8. The observed PXRD pattern (λ= 1.5401 Å) is shown in black, the calculated in red and the difference (observed - calculated) of both patterns is given in blue. The allowed reflection positions of the peaks are given as black and green (KCl) tics.

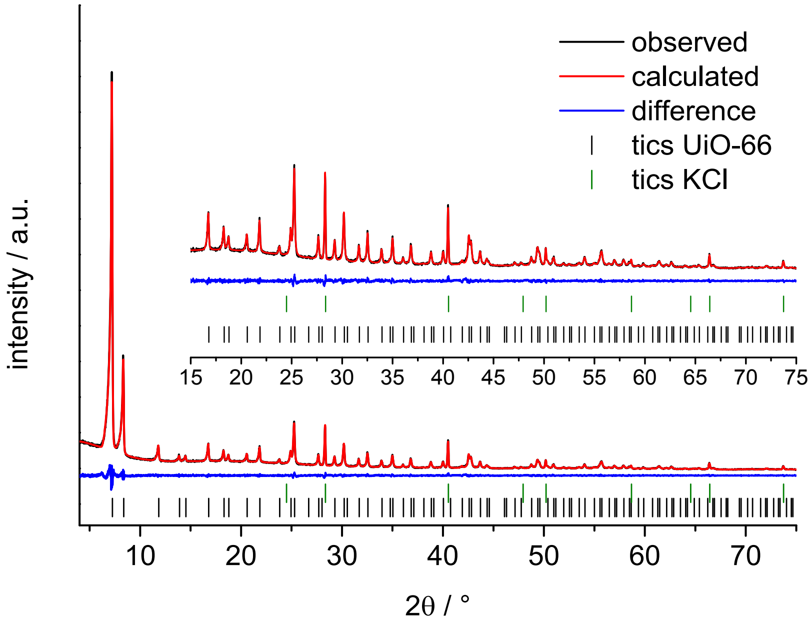

Fig. S9. Le Bail plot of UiO-66 sample P9. The observed PXRD pattern (λ= 1.5401 Å) is shown in black, the calculated in red and the difference (observed - calculated) of both patterns is given in blue. The allowed reflection positions of the peaks are given as black and green (KCl) tics.

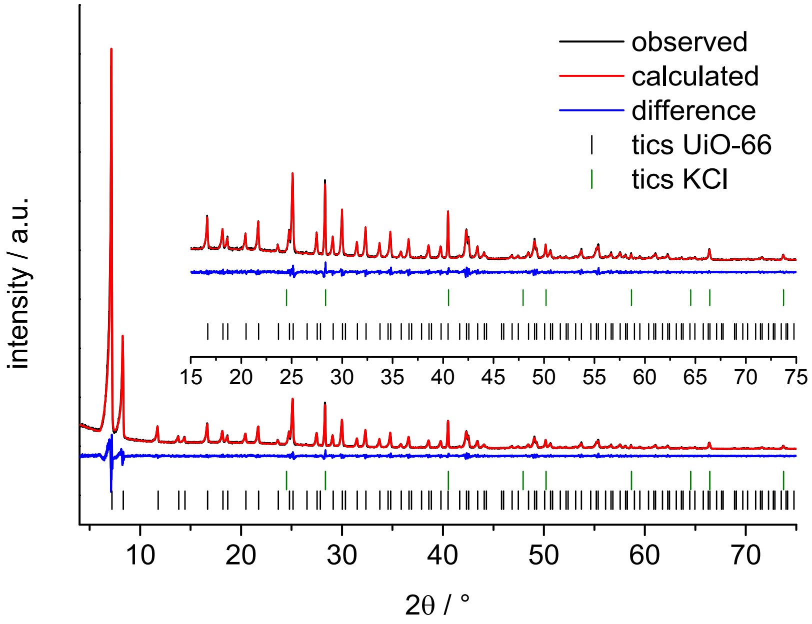

Fig. S10. Le Bail plot of UiO-66 sample P10. The observed PXRD pattern (λ= 1.5401 Å) is shown in black, the calculated in red and the difference (observed - calculated) of both patterns is given in blue. The allowed reflection positions of the peaks are given as black and green (KCl) tics.

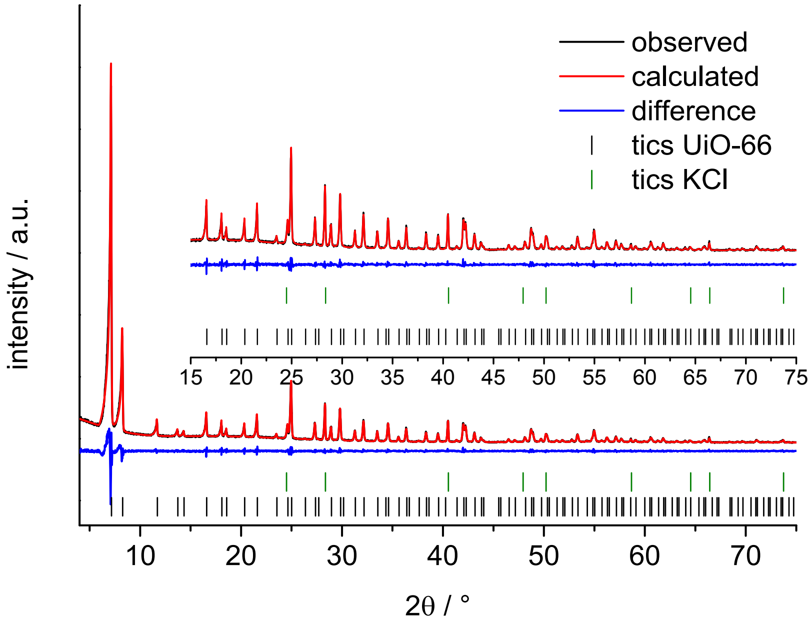

Fig. S11. Le Bail plot of UiO-66 sample P11. The observed PXRD pattern (λ= 1.5401 Å) is shown in black, the calculated in red and the difference (observed - calculated) of both patterns is given in blue. The allowed reflection positions of the peaks are given as black and green (KCl) tics.

Tab. S6. Results of the EDX analysis and comparison of the obtained lattice parameter for the bimetallic Ce/Zr-UiO-66 compounds using the Le Bail method and the calculated lattice parameters according the Vegard's Law.

Sample	**Ce / at%**	**Standard deviation / at%**	**$a_{Ce/Zr}$ [Å] calculated**	**$a_{Ce/Zr}$ [Å] obtained by Le Bail**
P1	8.3	1.1	20.8146	20.8028(8)
P2	15.4	0.6	20.8659	20.8636(7)
P3	17.9	0.6	20.8837	20.8714(6)
P4	20.6	0.7	20.9030	20.8988(4)
P5	22.4	0.5	20.9162	20.9198(4)
P6	26.5	0.9	20.9451	20.9469(5)
P7	34.1	0.8	20.9996	20.9867(4)
P8	40.7	0.6	21.0471	21.0329(3)
P9	50.6	0.6	21.1184	21.1022(3)
P10	65.6	0.5	21.2259	21.2282(4)
P11	78.9	1.3	21.3214	21.3511(3)

2.3. Thermal stability

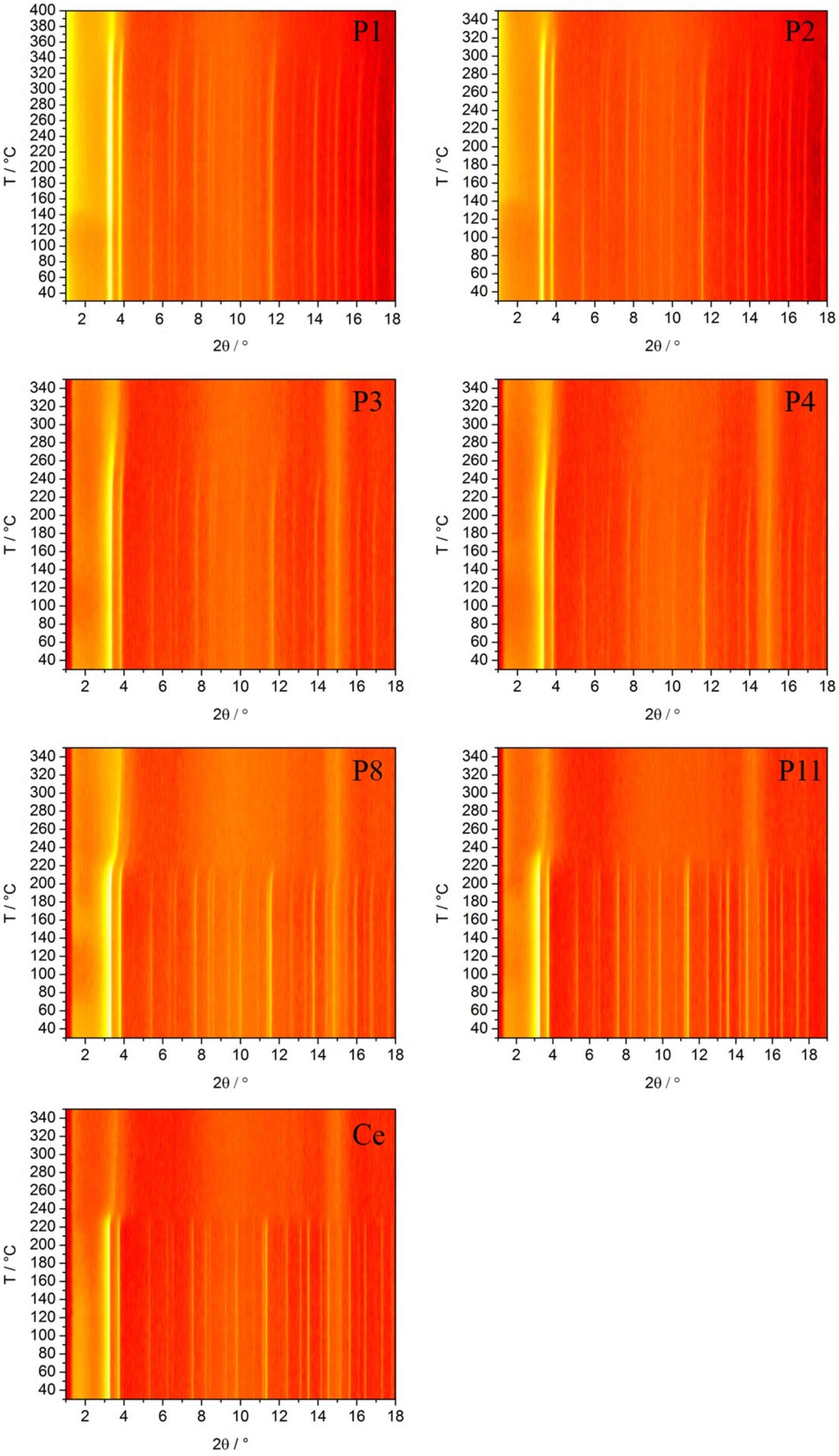

Fig. S12. Results of the VT-PXRD measurement of selected Ce/Zr-UiO-66 compounds and pure Ce-UiO-66 (λ = 0.7093 Å) in top view.

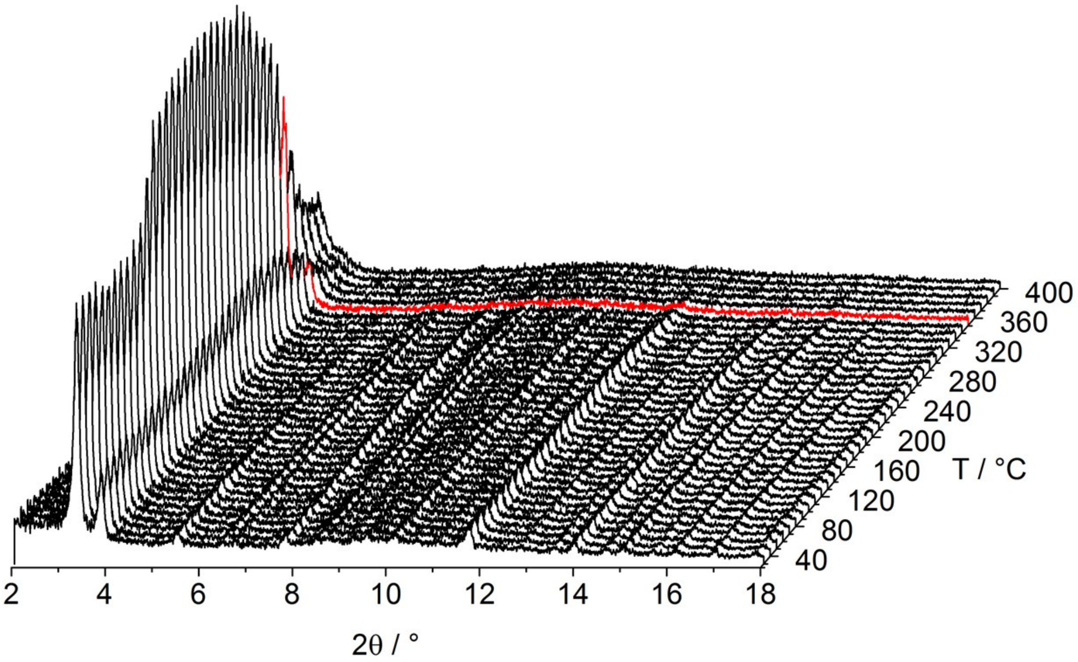

Fig. S13. Results of the VT-PXRD measurement (λ = 0.7093 Å) of UiO-66 sample P1. The red PXRD pattern marks the temperature (350 °C) to which the compound is stable.

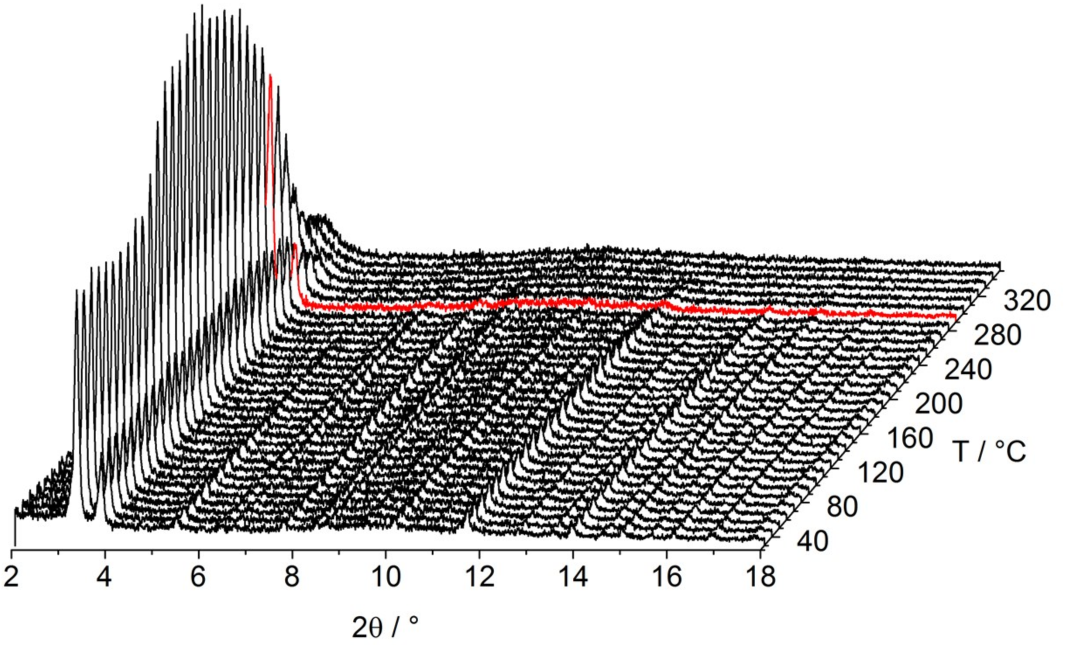

Fig. S14. Results of the VT-PXRD measurement (λ = 0.7093 Å) of UiO-66 sample P2. The red PXRD pattern marks the temperature (350 °C) to which the compound is stable.

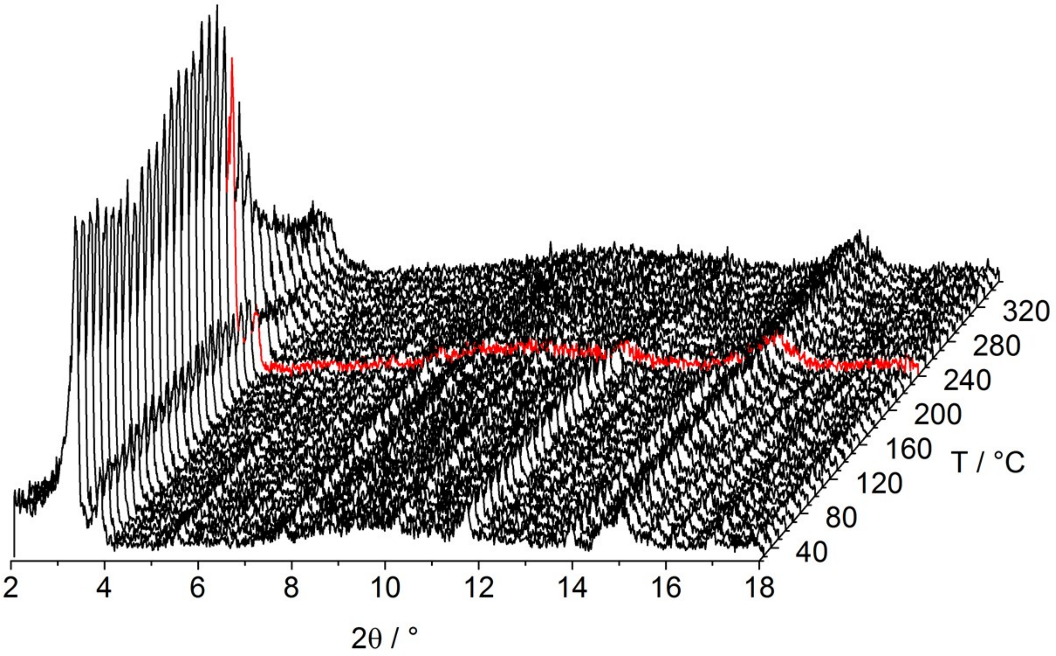

Fig. S15. Results of the VT-PXRD measurement (λ = 0.7093 Å) of UiO-66 sample P3. The red PXRD pattern marks the temperature (350 °C) to which the compound is stable.

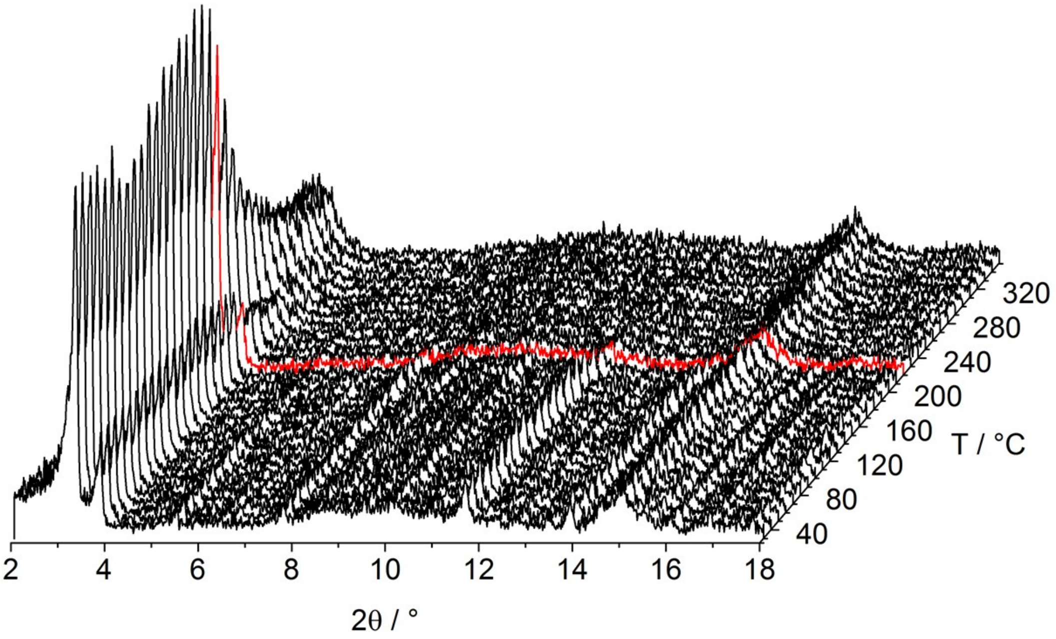

Fig. S16. Results of the VT-PXRD measurement (λ = 0.7093 Å) of UiO-66 sample P4. The red PXRD pattern marks the temperature (350 °C) to which the compound is stable.

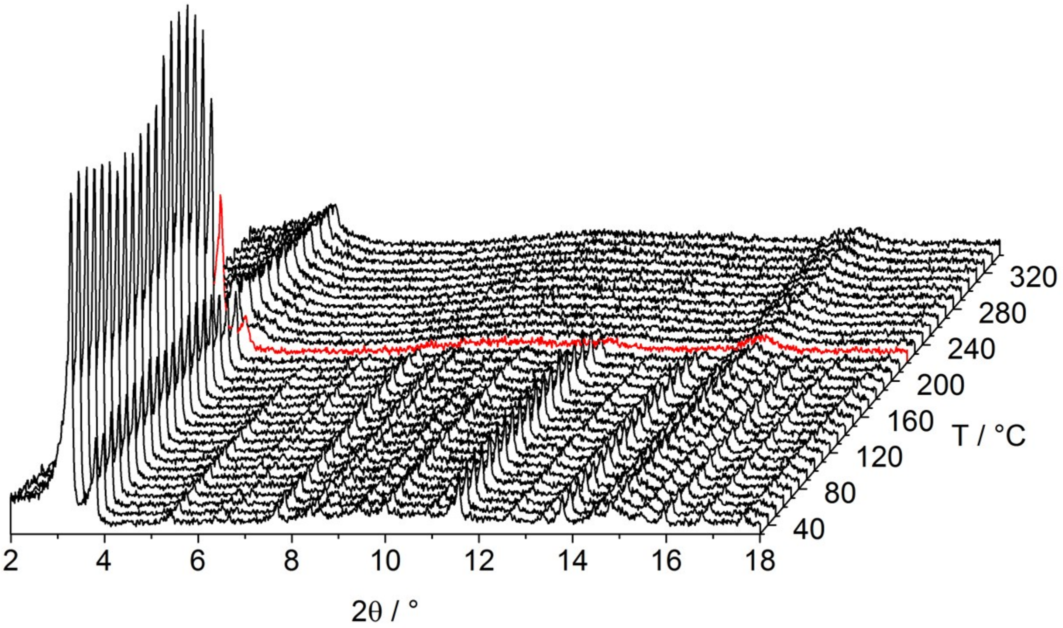

Fig. S17. Results of the VT-PXRD measurement (λ = 0.7093 Å) of UiO-66 sample P8. The red PXRD pattern marks the temperature (350 °C) to which the compound is stable.

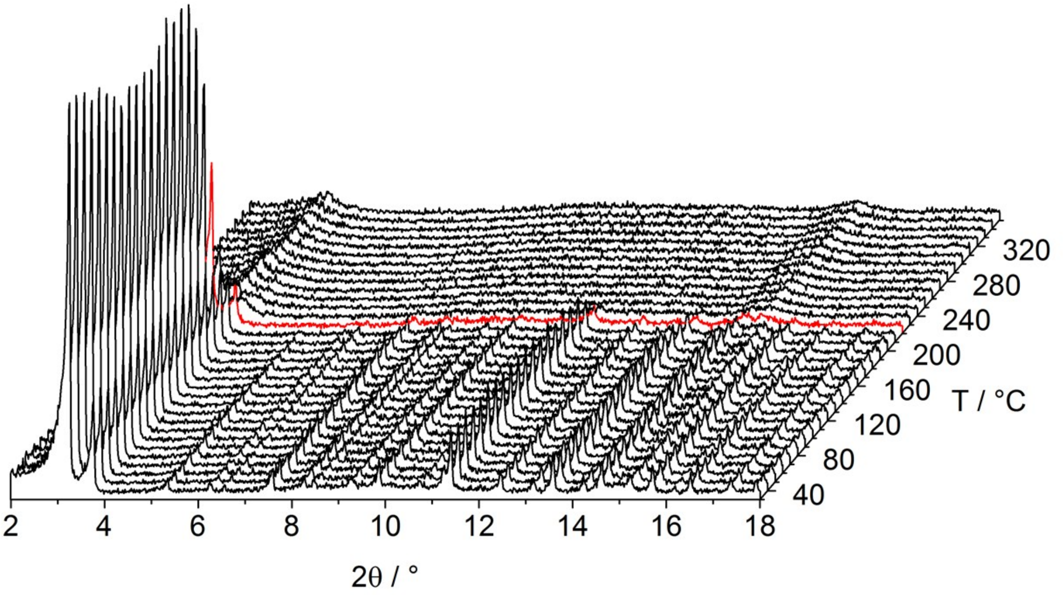

Fig. S18. Results of the VT-PXRD measurement (λ = 0.7093 Å) of UiO-66 sample P11. The red PXRD pattern marks the temperature (350 °C) to which the compound is stable.

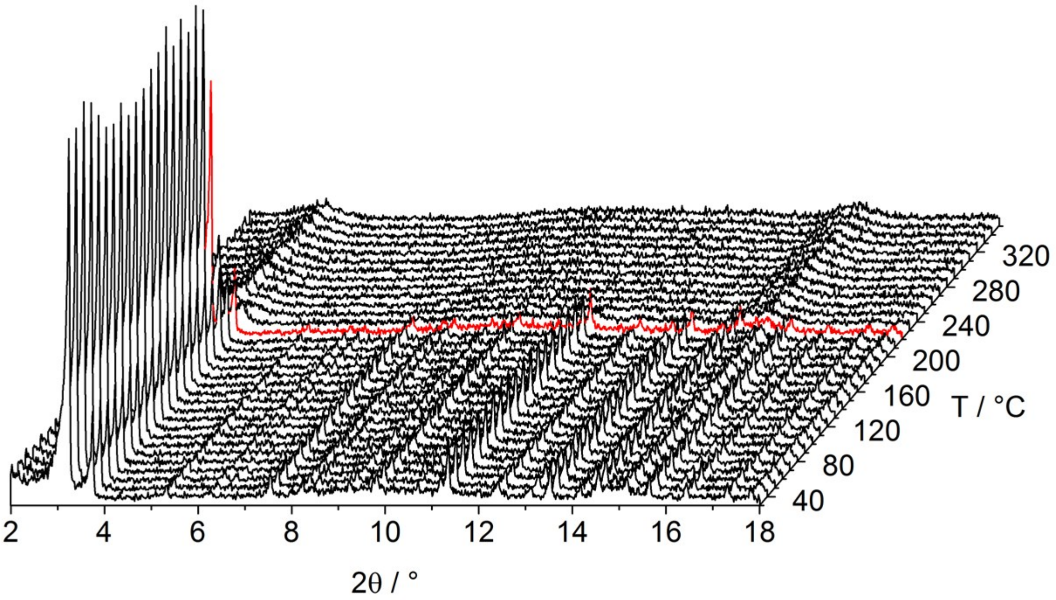

Fig. S19. Results of the VT-PXRD measurement (λ = 0.7093 Å) of pure Ce-UiO-66. The red PXRD pattern marks the temperature (350 °C) to which the compound is stable.

Tab. S7. Thermal stabilities of the Ce/Zr-UiO-66 compounds obtained by VT-PXRD.

Sample	**Ce / at%**	**Thermal Stability / °C**
P1	8.3(±1.1)	350(±5)
P2	15.4(±0.6)	290(±5)
P3	17.9(±0.6)	250(±5)
P4	20.6(±0.7)	230(±5)
P8	40.7(±0.6)	220(±5)
P11	78.9(±1.3)	220(±5)

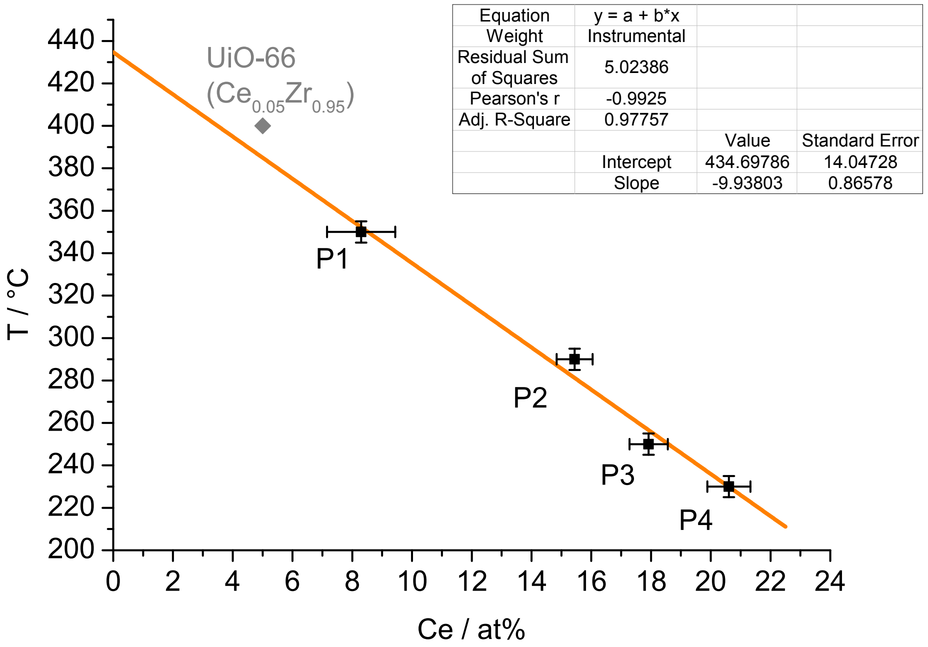

Equation	y = a + b*x		
Weight	Instrumental		
Residual Sum of Squares	5.02386		
Pearson's r	-0.9925		
Adj. R-Square	0.97757		
		Value	Standard Error
	Intercept	434.69786	14.04728
	Slope	-9.93803	0.86578

Fig. S20. Linear regression of the thermal stability for the bimetallic Ce/Zr-UiO-66 compounds P1-4 with Ce amount lower than 20.6 at%. The grey diamond marks the thermal stability (measured by TGA) of the UiO-66($Ce_{0.05}Zr_{0.95}$) published by Nouar et al.[4]

2.4. pH stability

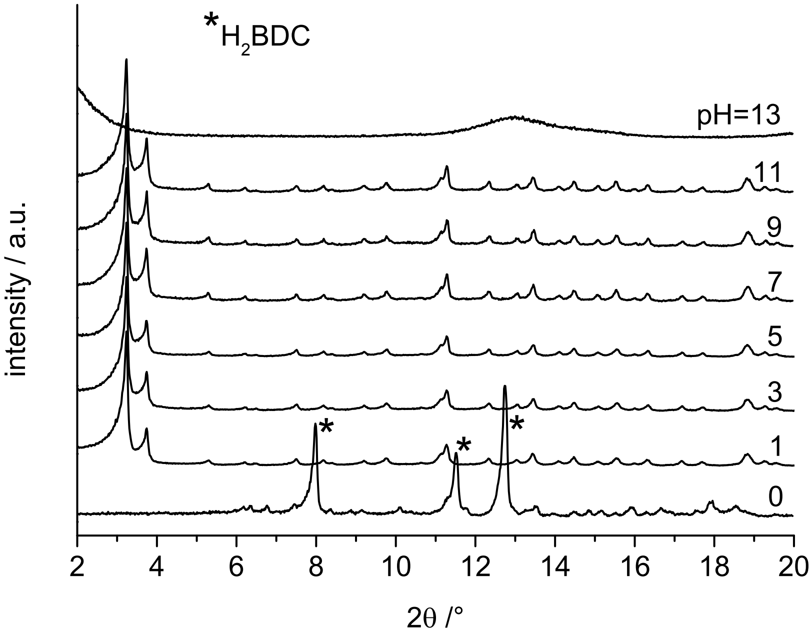

Fig. S21. PXRD patterns (λ = 0.7093 Å) of Ce-UiO-66 after stirring in acidic (HCl) and basic (NaOH) solutions in the range pH = 0-13. At pH = 0, the sample dissolves and terephthalic acid (H_2BDC) recrystallizes.

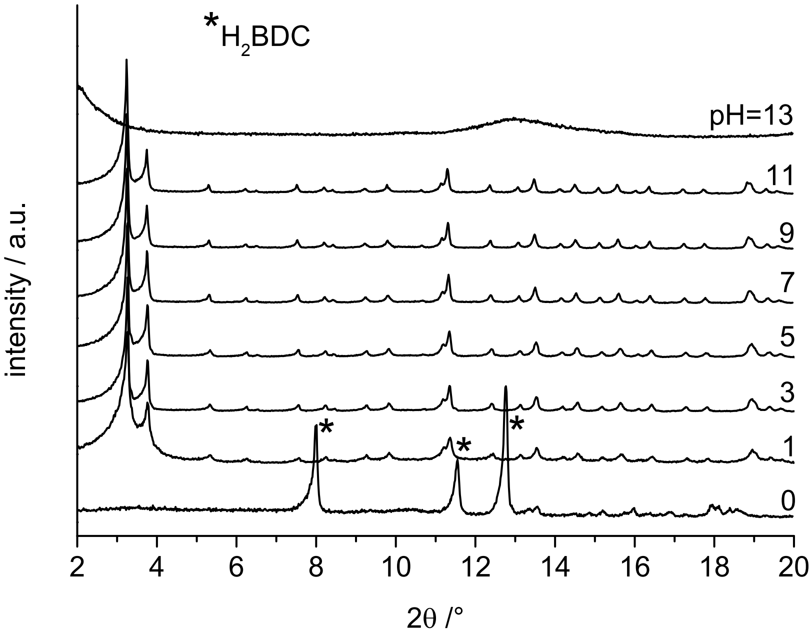

Fig. S22. PXRD patterns (λ = 0.7093 Å) of UiO-66 sample P11 after stirring for 24 h in acidic (HCl) and basic (NaOH) solutions in the range pH = 0-13. At pH = 0, the sample dissolves and terephthalic acid (H_2BDC) recrystallizes.

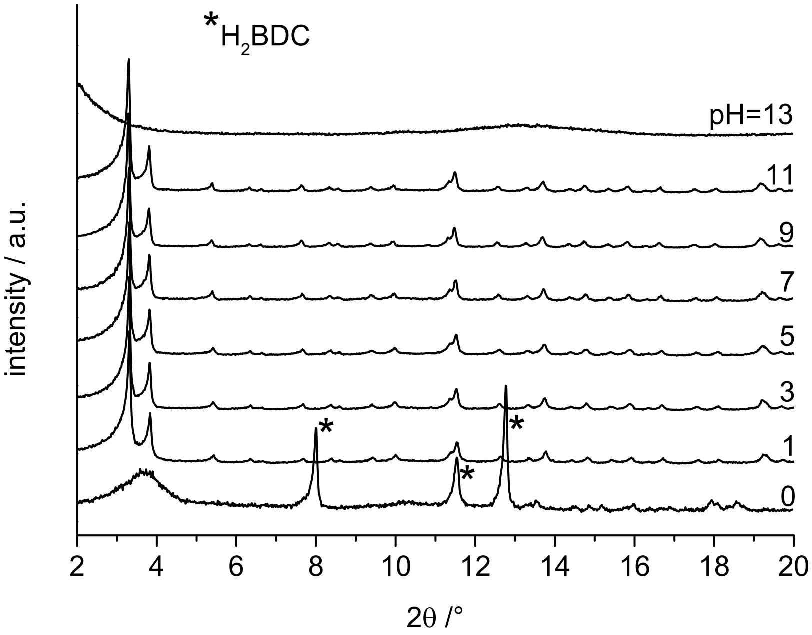

Fig. S23. PXRD patterns (λ = 0.7093 Å) of UiO-66 sample P8 after stirring for 24 h in acidic (HCl) and basic (NaOH) solutions in the range pH = 0-13. At pH = 0, the sample dissolves and terephthalic acid (H_2BDC) recrystallizes.

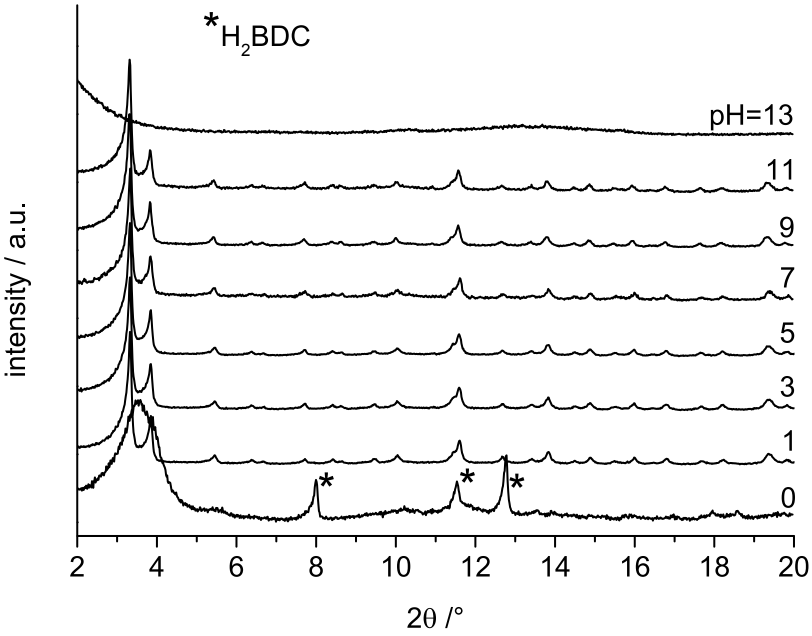

Fig. S24. PXRD patterns (λ = 0.7093 Å) of UiO-66 sample P4 after stirring for 24 h in acidic (HCl) and basic (NaOH) solutions in the range pH = 0-13. At pH = 0, the sample dissolves and terephthalic acid (H_2BDC) recrystallizes.

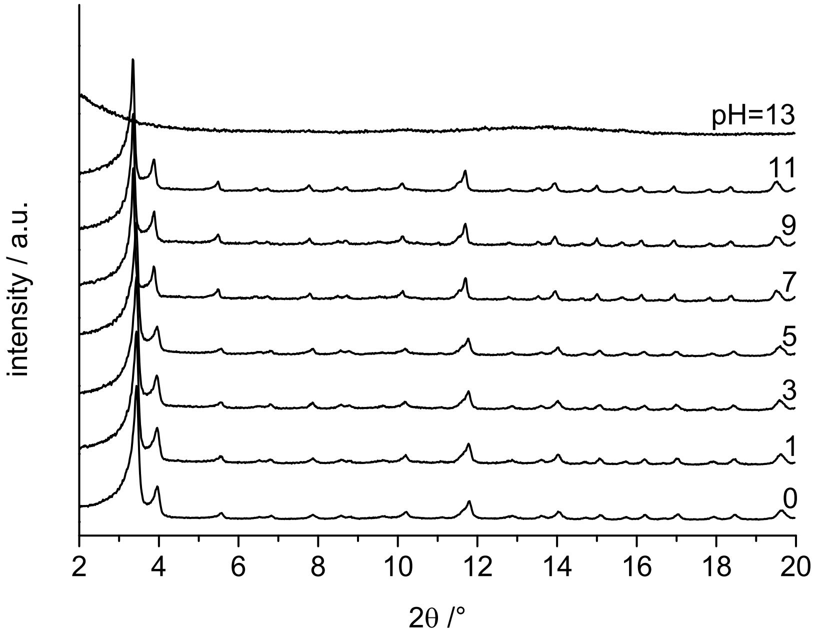

Fig. S25. PXRD patterns (λ = 0.7093 Å) of Zr-UiO-66 after stirring for 24 h in acidic (HCl) and basic (NaOH) solutions in the range pH = 0-13.

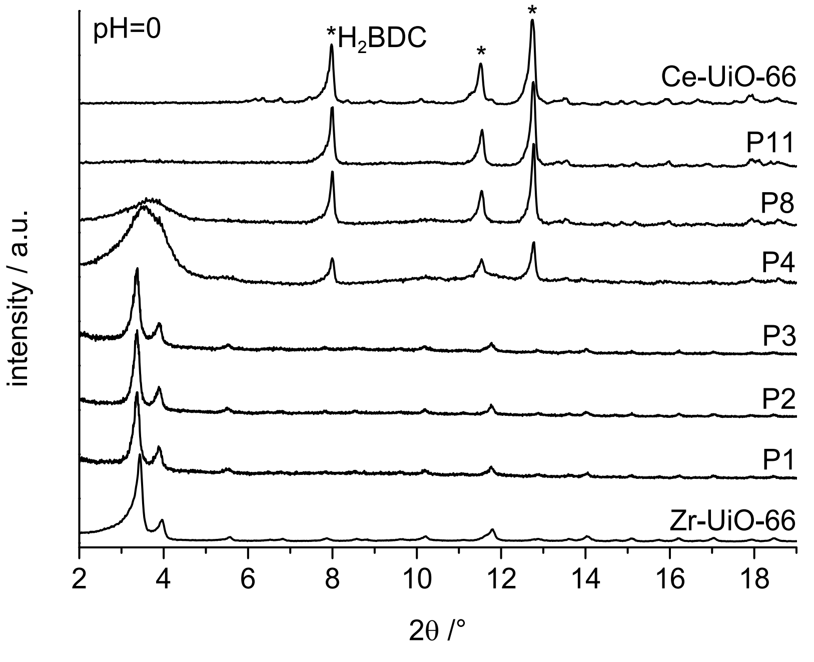

Fig. S26. PXRD patterns (λ = 0.7093 Å) of the pure Ce- und Zr-UiO-66 and the bimetallic Ce/Zr-UiO-66 compounds after stirring for 24 h in 1M HCl (pH=0). At pH = 0, the samples P4, P8, P11 and Ce-UiO-66 dissolve and terephthalic acid (H_2BDC) recrystallizes.

2.5. Thermogravimetric analysis

Tab. S8. Summary of the results of the thermogravimetric experiments on the bimetallic Ce/Zr-UiO-66 compounds. Comparison of the observed weight loss Δm_2 (obs.) for the decomposition of the organic linker molecules with the calculated weight loss Δm_2 (calcd.).

Sample	M_{MOF} / g mol^{-1}	M_{Oxide} / g mol^{-1}	Δm_1 / % (obs.)	Δm_2 / % (obs.)	Δm_2 / % (calcd.)	Δm_2 (calcd.) - Δm_2 (obs.)	m_{Oxide} / %	$T_{Decomposition}$ / °C
P1	1688	764	34.4	34.4	37.7	-3.3	31.2	> 360
P2	1708	783	36.5	33.7	35.2	-1.5	29.8	> 360
P3	1718	793	34.0	34.7	36.5	-1.8	31.3	> 350
P4	1723	798	35.0	35.3	34.4	+1.1	29.7	> 340
P8	1781	857	32.8	34.3	35.5	-1.2	32.9	> 300
P11	1894	969	34.9	32.5	31.1	+1.4	32.6	> 300

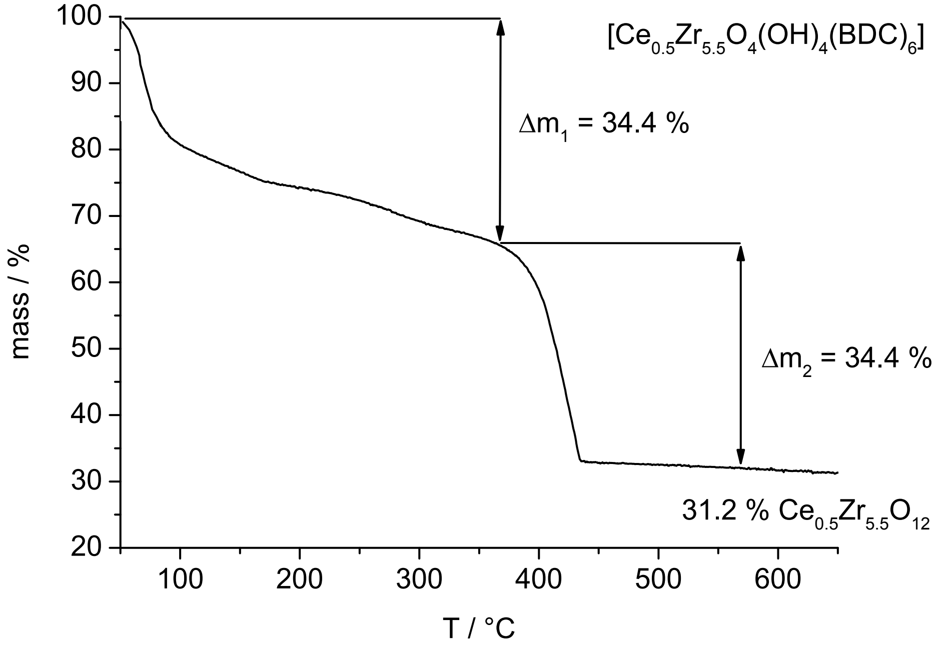

Fig. S27. TG curve of UiO-66 sample P1 heated under air flow.

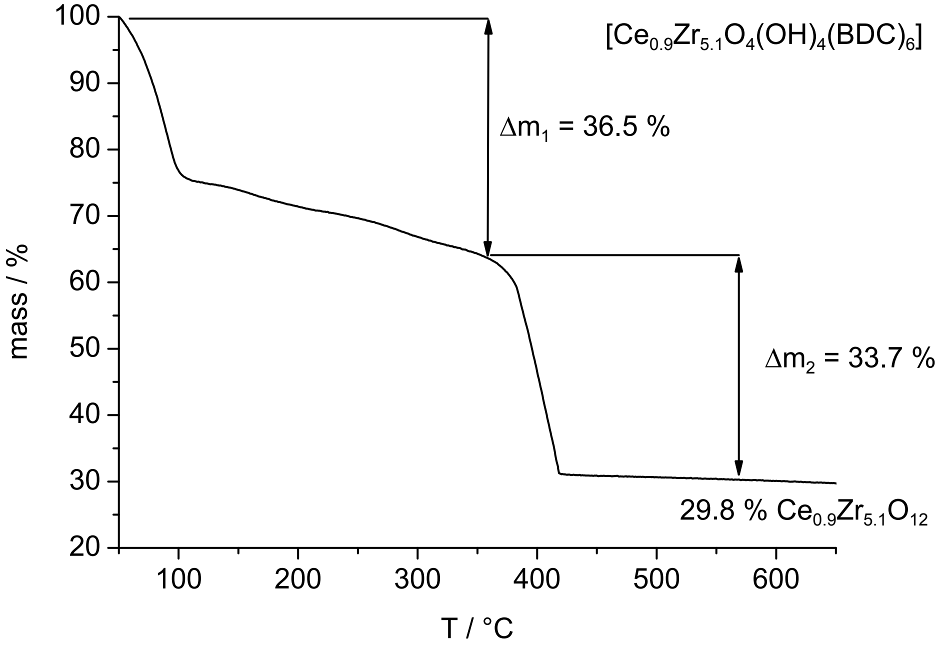

Fig. S28. TG curve of UiO-66 sample P2 heated under air flow.

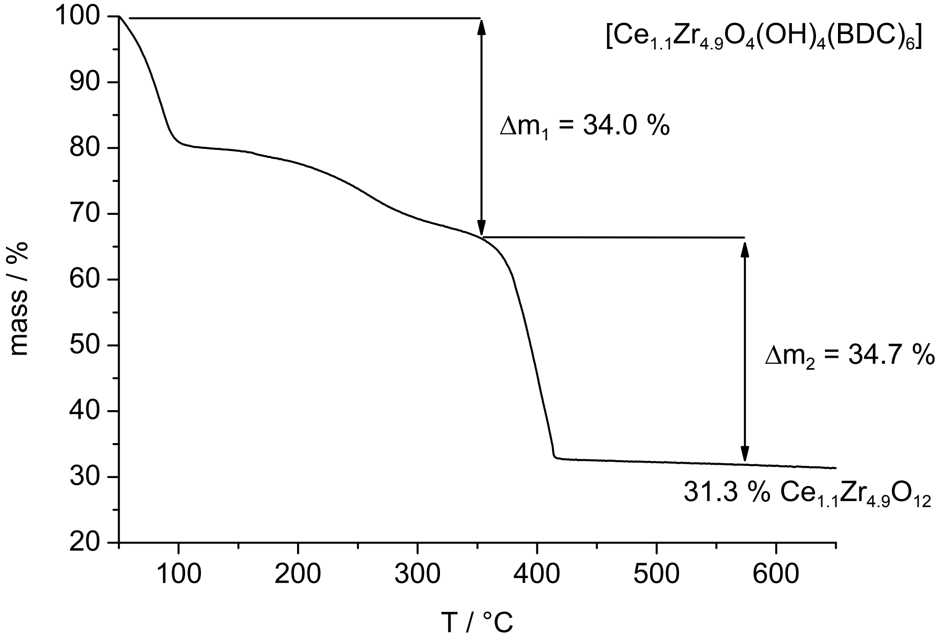

Fig. S29. TG curve of UiO-66 sample P3 heated under air flow.

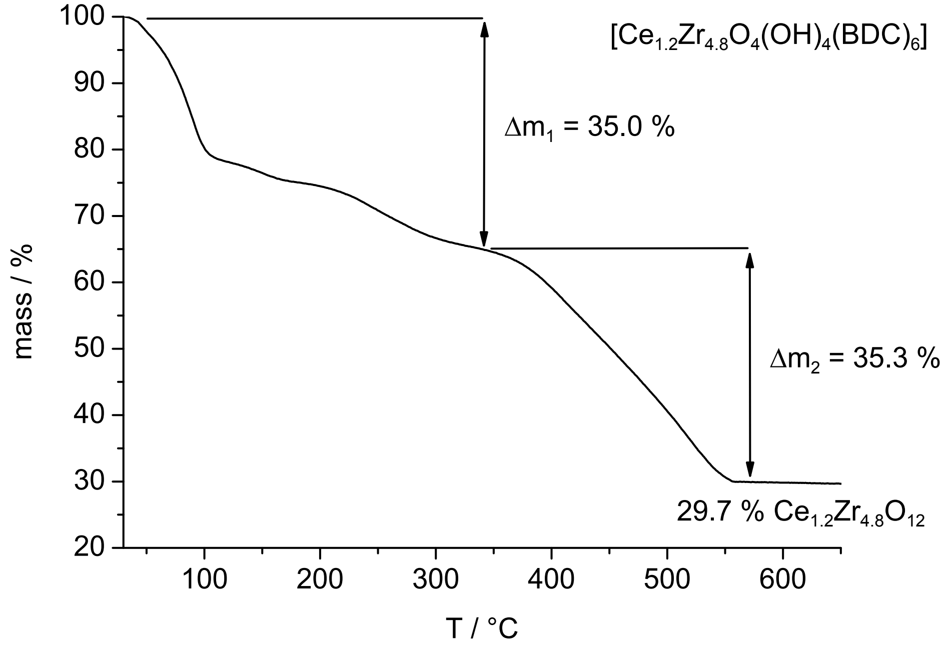

Fig. S30. TG curve of UiO-66 sample P4 heated under air flow.

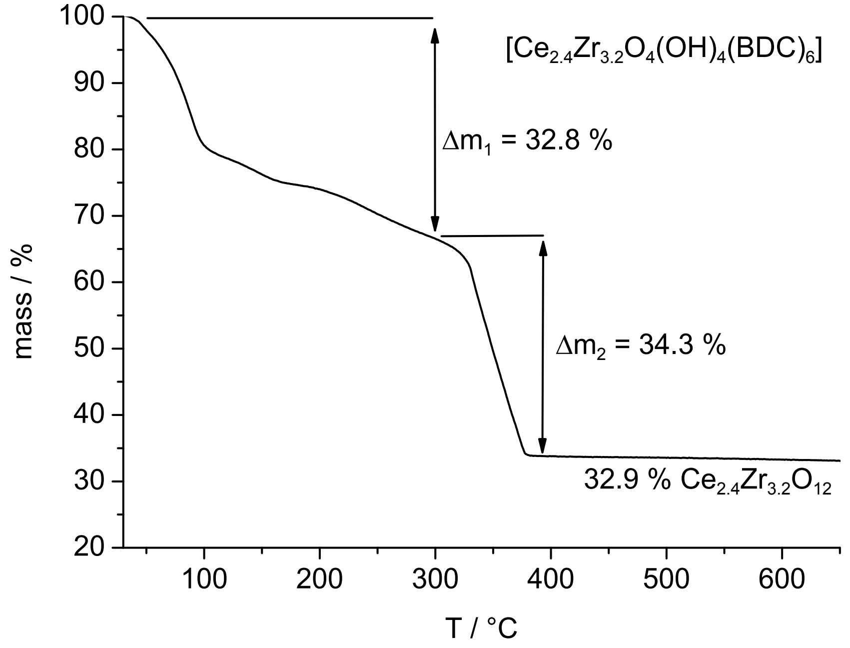

Fig. S31. TG curve of UiO-66 sample P8 heated under air flow.

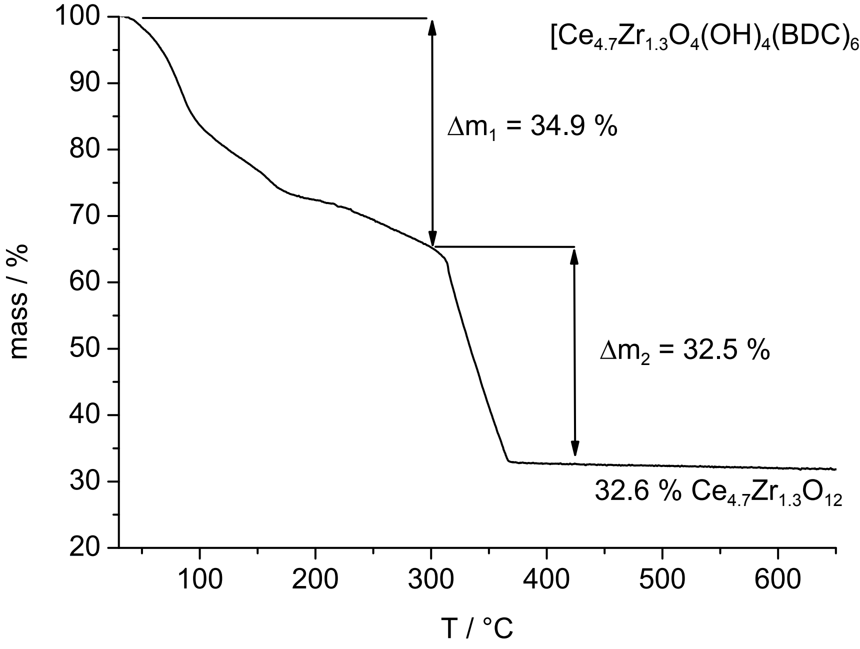

Fig. S32. TG curve of UiO-66 sample P11 heated under air flow.

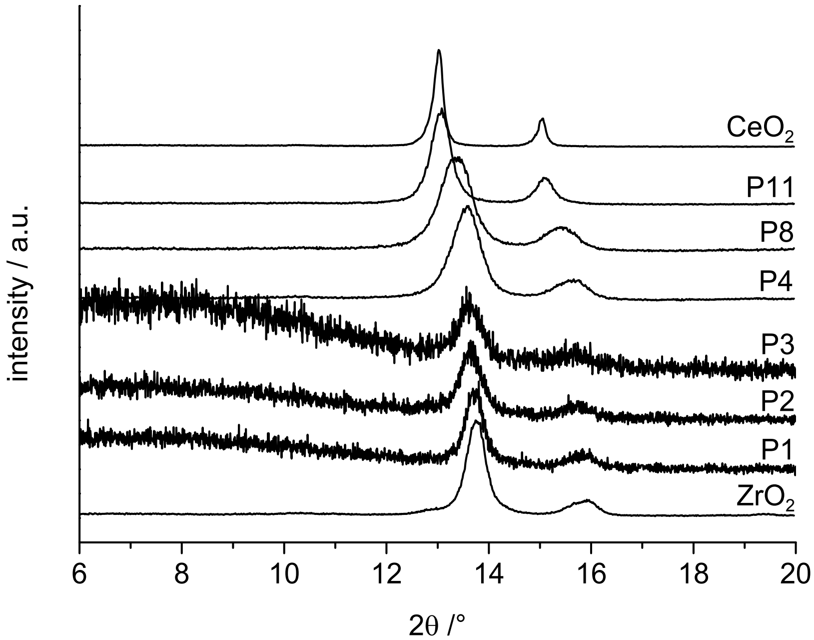

Fig. S33. Comparison of the PXRD patterns of the bimetallic Ce/Zr-UiO-66 compounds after the thermogravimetric analysis (650°C). The low signal to noise ratio in the PXRD patterns of P1, P2 and P3 are due to very small residue amounts.

2.6. N$_2$ sorption measurements

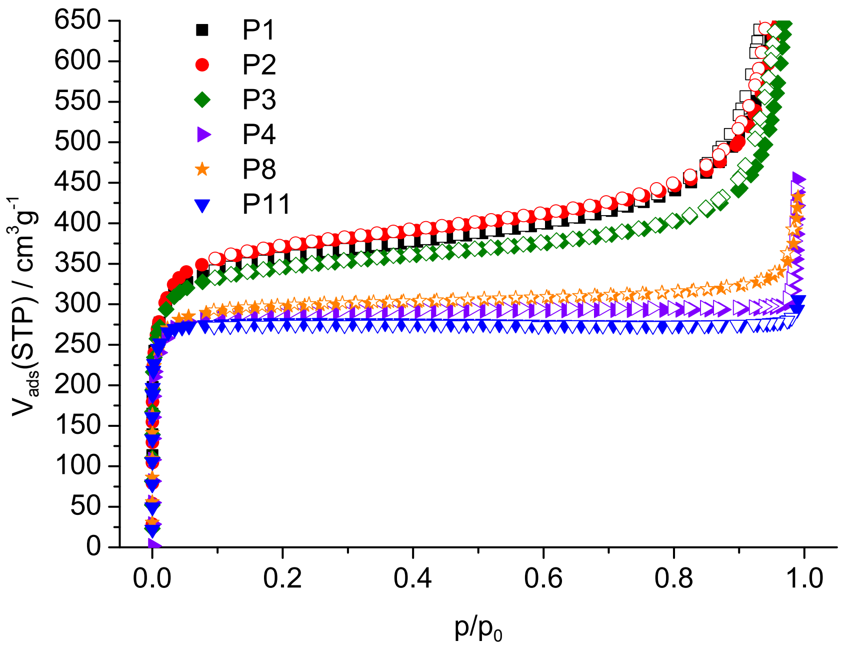

Fig. S34. Results of N$_2$ sorption measurements of activated (160 °C, 10^{-2} kPa) Ce/Zr-UiO-66 compounds. Filled symbols mark the adsorption, while empty symbols mark the desorption step.

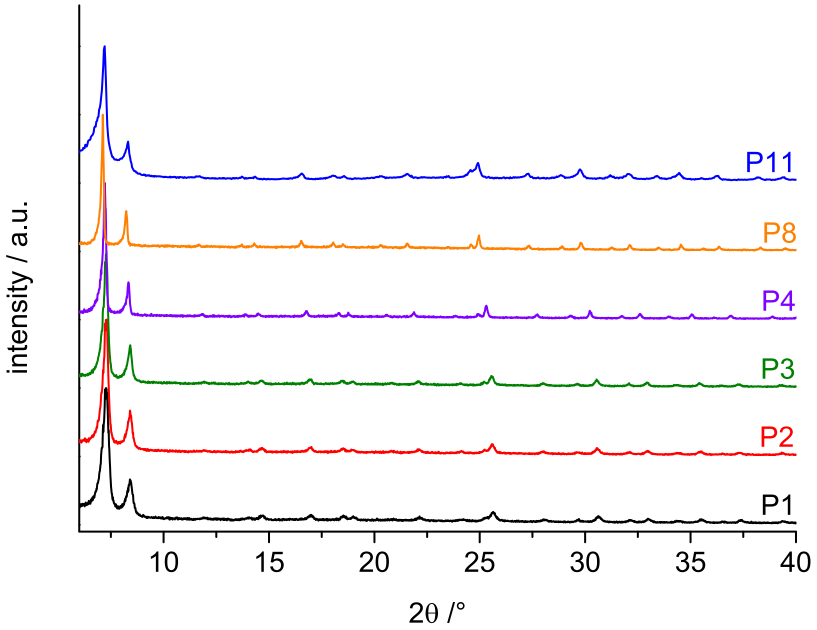

Fig. S35. PXRD patterns (λ= 1.5406 Å) of Ce/Zr-UiO-66 compounds after the N$_2$ sorption measurement.

2.7. DLS measurements

Tab. S9. Results of the DLS measurement. The hydrodynamic diameter (d_H) and the Polydispersity Index (PI) for the mixed-metal UiO-66 compounds are given.

Sample	d_H / nm	PI
P1	157(41)	0.192
P2	152(19)	0.153
P3	169(25)	0.098
P4	214(28)	0.159
P8	247(7)	0.103
P11	407(18)	0.143

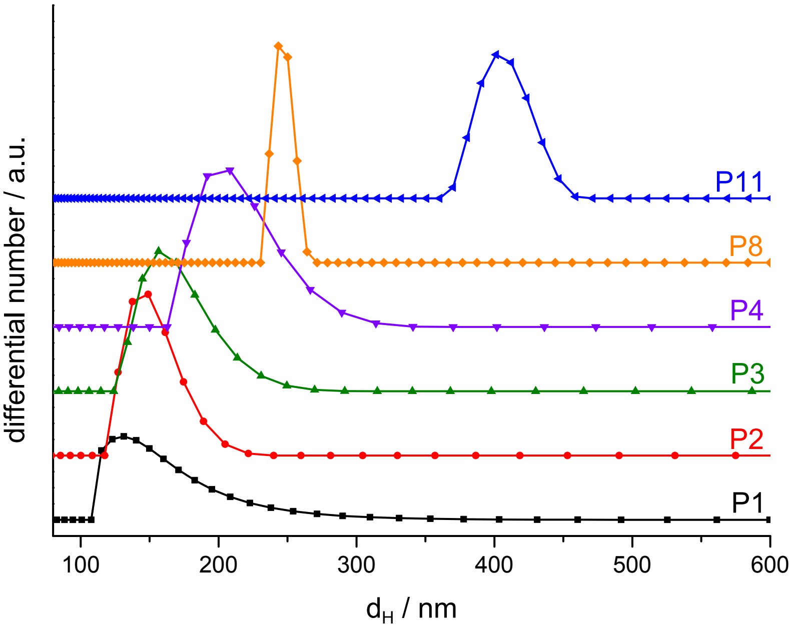

Fig. S36. Differential number distribution of the bimetallic Ce/Zr-UiO-66 compounds dispersed in ethanol.

3.0. Characterization of Ce/Zr-MOF-808

3.1. Results of the EDX analyses

Tab. S10: Results of the EDX analysis of the bimetallic Ce/Zr-MOF-808 compounds.

Sample	Elements	1. / at%	2. / at%	3. / at%	4. / at%	Mean value / at%	Standard deviation / at%
M1	Zr	80.46	79.23	81.39	80.69	80.4	0.2
	Ce	19.54	20.77	18.61	19.31	19.6	0.2
M2	Zr	67.51	69.72	68.45	68.65	68.6	0.3
	Ce	32.49	30.28	31.55	31.35	31.4	0.3
M3	Zr	60.12	59.10	60.24	59.94	59.9	0.4
	Ce	39.88	40.90	39.76	40.06	40.1	0.4
M4	Zr	47.21	45.48	45.97	46.26	46.2	0.5
	Ce	52.79	54.52	54.03	53.74	53.8	0.5
M5	Zr	32.25	31.38	31.03	31.20	31.5	0.7
	Ce	67.75	68.62	68.97	68.80	68.5	0.7

Tab. S11. Comparison of the molar ratio of Ce:Zr used for the synthesis of mixed-metal Ce/Zr-MOF-808 with composition [$Ce_xZr_yO_4(OH)_4(BTC)_2(OH)_6(H_2O)_6$] and measured by EDX analysis.

Sample	Ce_x:Zr_y [at%] measured by EDX	Ce_x:Zr_y calculated from EDX	Ce_x:Zr_y used for synthesis
M1	19.6 : 80.4	1.2 : 4.8	1.0 : 5.0
M2	31.4 : 68.8	1.9 : 4.1	2.0 : 4.0
M3	40.1 : 59.9	2.4 : 3.6	3.0: 3.0
M4	53.8 : 46.2	3.2 : 2.8	4.0 : 2.0
M5	68.5 : 31.5	4.1 : 1.9	5.0 : 1.0

3.2. Powder X-ray diffraction

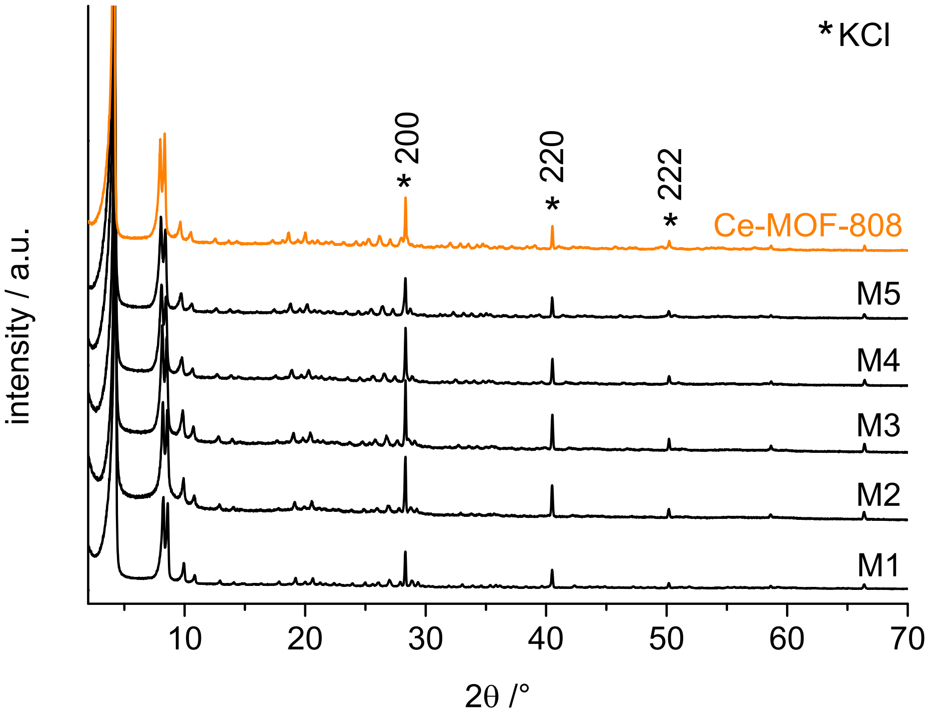

Fig. S37. PXRD patterns of the bimetallic Ce/Zr-MOF-808 compounds in comparison with a PXRD pattern of pure Ce-MOF-808. KCl was added as internal standard and for simpler comparison. Reflection positions of KCl are marked by asterisks.

Tab. S12. Lattice parameters of the bimetallic Ce/Zr-MOF-808 compounds obtained by Le Bail profile fitting with KCl (*a*= 6.2890(2) Å) as internal standard.

Sample	**SG**	**λ [Å]**	***a* [Å]**	**R_{wp} /%**	**GoF**
M1	$Fd\bar{3}m$	1.5401	35.366(1)	6.27	2.86
M2	$Fd\bar{3}m$	1.5401	35.483(4)	5.75	2.20
M3	$Fd\bar{3}m$	1.5401	35.726(3)	5.32	2.05
M4	$Fd\bar{3}m$	1.5401	35.968(3)	6.99	2.43
M5	$Fd\bar{3}m$	1.5401	36.127(2)	6.66	2.34

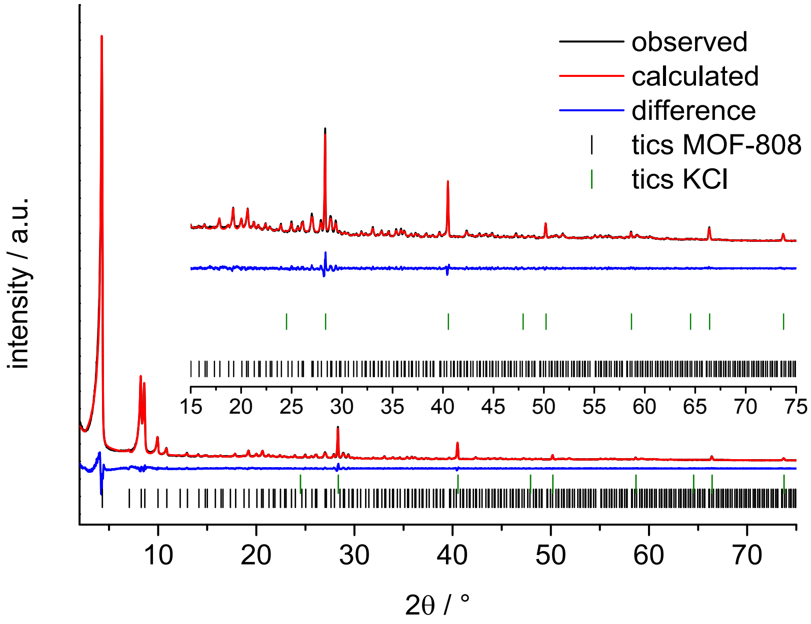

Fig. S38. Le Bail plot of MOF-808 sample M1. The observed PXRD pattern (λ= 1.5401 Å) is shown in black, the calculated in red and the difference (observed - calculated) of both patterns is given in blue. The allowed reflection positions of the peaks are given as black and green (KCl) tics.

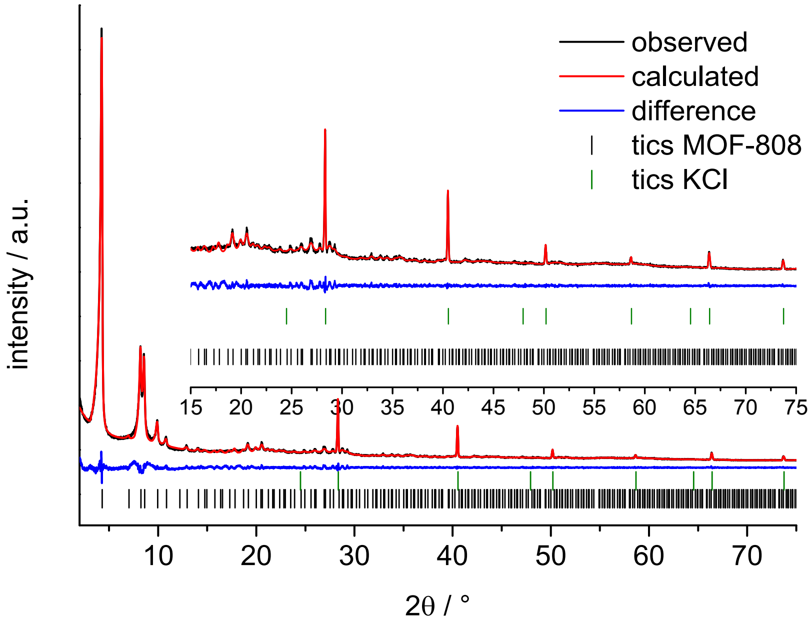

Fig. S39. Le Bail plot of MOF-808 sample M2. The observed PXRD pattern (λ= 1.5401 Å) is shown in black, the calculated in red and the difference (observed - calculated) of both patterns is given in blue. The allowed reflection positions of the peaks are given as black and green (KCl) tics.

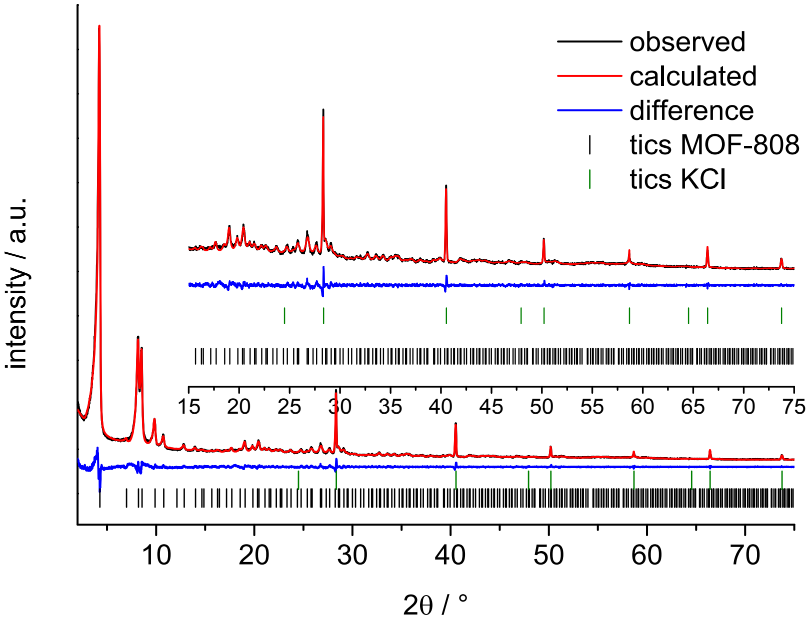

Fig. S40. Le Bail plot of MOF-808 sample M3. The observed PXRD pattern (λ= 1.5401 Å) is shown in black, the calculated in red and the difference (observed - calculated) of both patterns is given in blue. The allowed reflection positions of the peaks are given as black and green (KCl) tics.

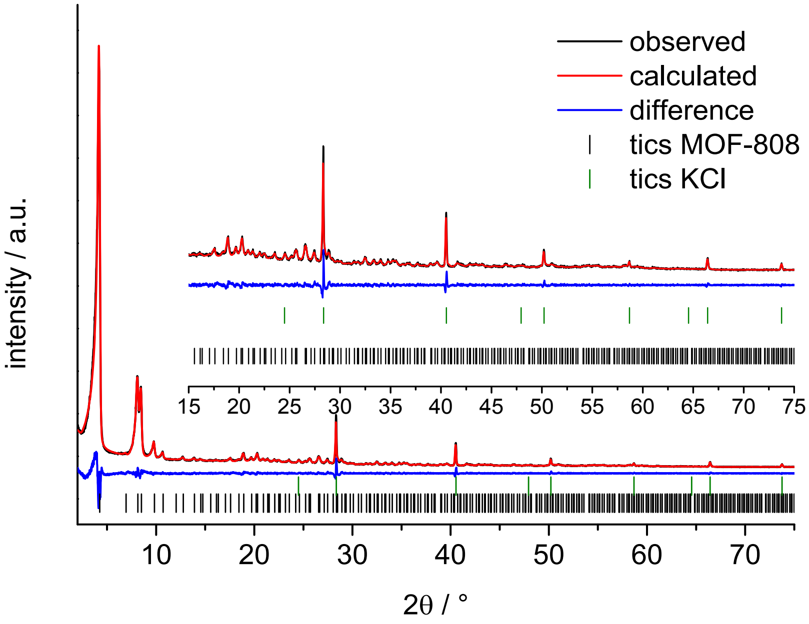

Fig. S41. Le Bail plot of MOF-808 sample M4. The observed PXRD pattern (λ= 1.5401 Å) is shown in black, the calculated in red and the difference (observed - calculated) of both patterns is given in blue. The allowed reflection positions of the peaks are given as black and green (KCl) tics.

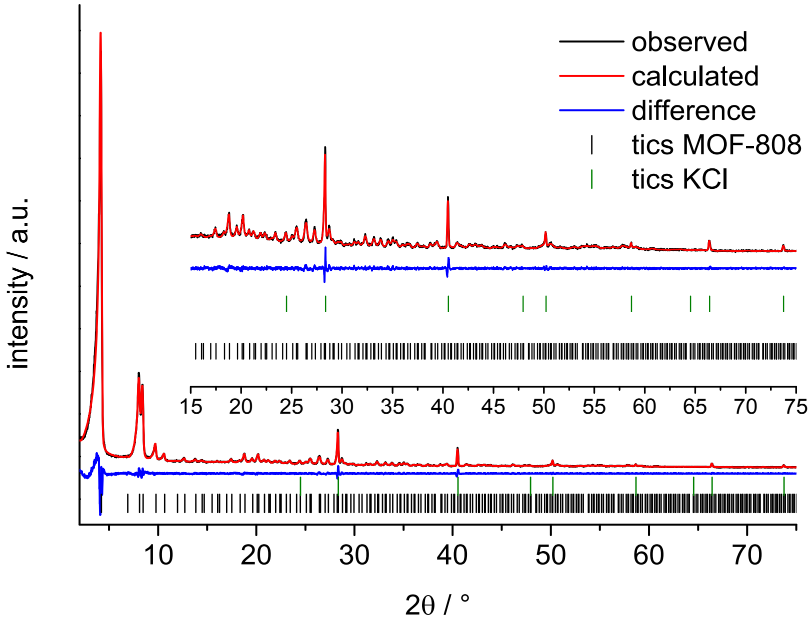

Fig. S42. Le Bail plot of MOF-808 sample M5. The observed PXRD pattern (λ= 1.5401 Å) is shown in black, the calculated in red and the difference (observed - calculated) of both patterns is given in blue. The allowed reflection positions of the peaks are given as black and green (KCl) tics.

Tab. S13. Results of the EDX analysis and comparison of the obtained lattice parameter for the bimetallic Ce/Zr-MOF-808 compounds using the Le Bail method and the calculated lattice parameters according the Vegard's Law.

Sample	**Ce / at%**	**Standard deviation / at%**	$a_{Ce/Zr}$ **[Å] calculated**	$a_{Ce/Zr}$ **[Å] obtained by Le Bail**
Zr-MOF-808[5]	0	-	35.076	-
M1	19.6	0.2	35.382	35.366(1)
M2	31.4	0.3	35.508	35.483(4)
M3	40.1	0.4	35.628	35.726(3)
M4	53.8	0.5	35.823	35.968(3)
M5	68.5	0.7	36.019	36.127(2)
Ce-MOF-808[6]	100	-	36.451	-

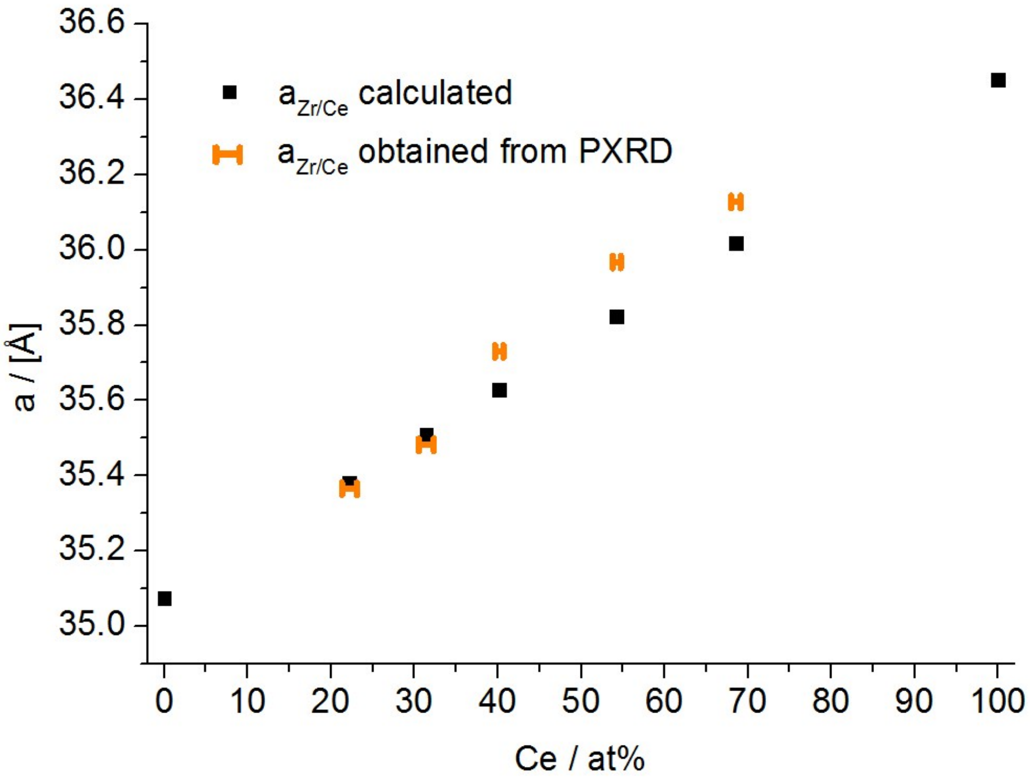

Fig. S43. Lattice parameters of Ce/Zr-MOF-808 calculated according the Vegard's Law in comparison with the lattice parameters obtained by the Le Bail method and using KCl as internal standard.

3.3. Thermal stability

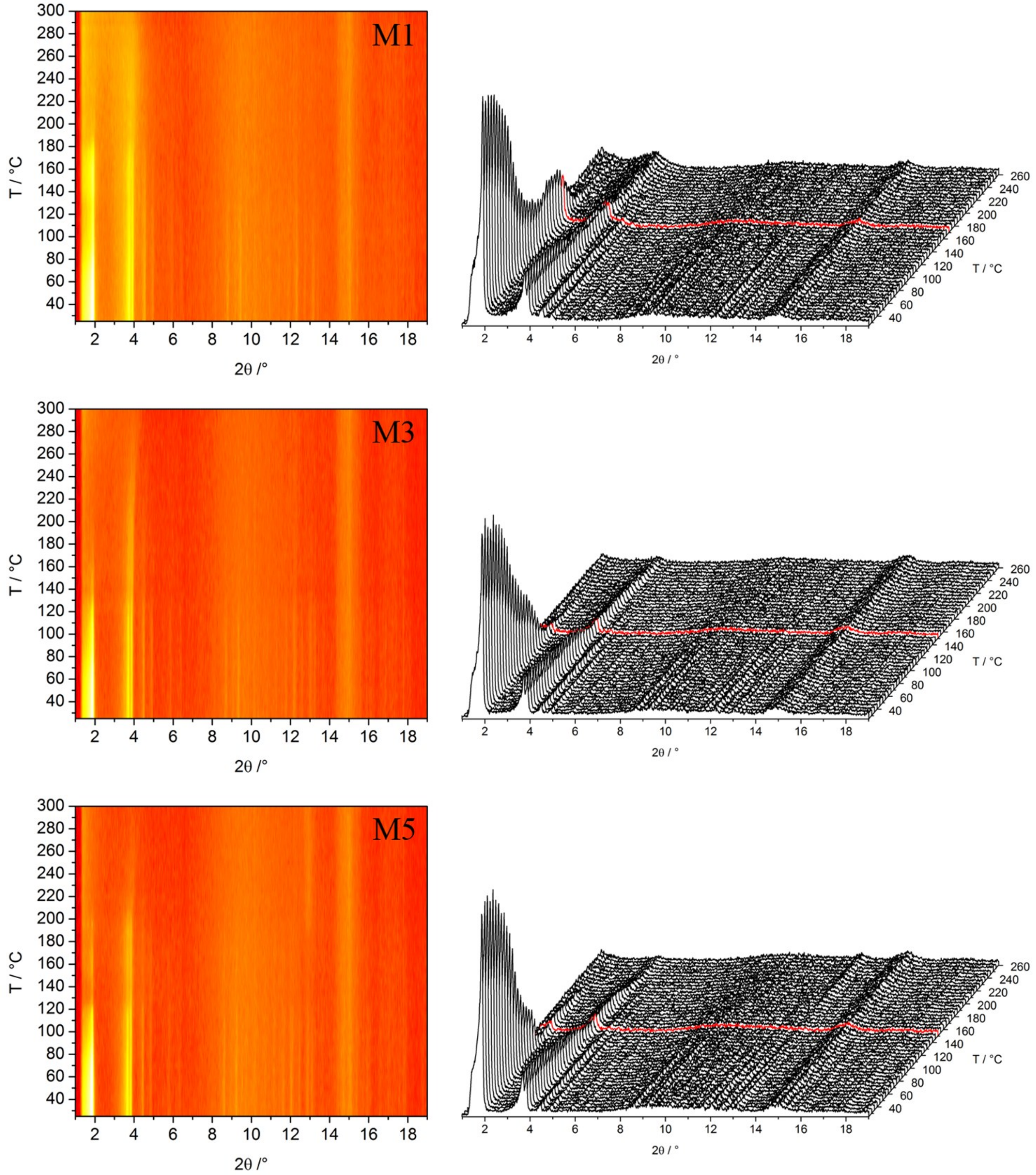

Fig. S44. Results of the VT-PXRD measurement of the mixed-metal Ce/Zr-MOF-808 compounds (λ = 0.7093 Å) in top view (left). The red PXRD pattern marks the temperature to which the compounds are stable (right).

3.4. N$_2$ sorption measurements

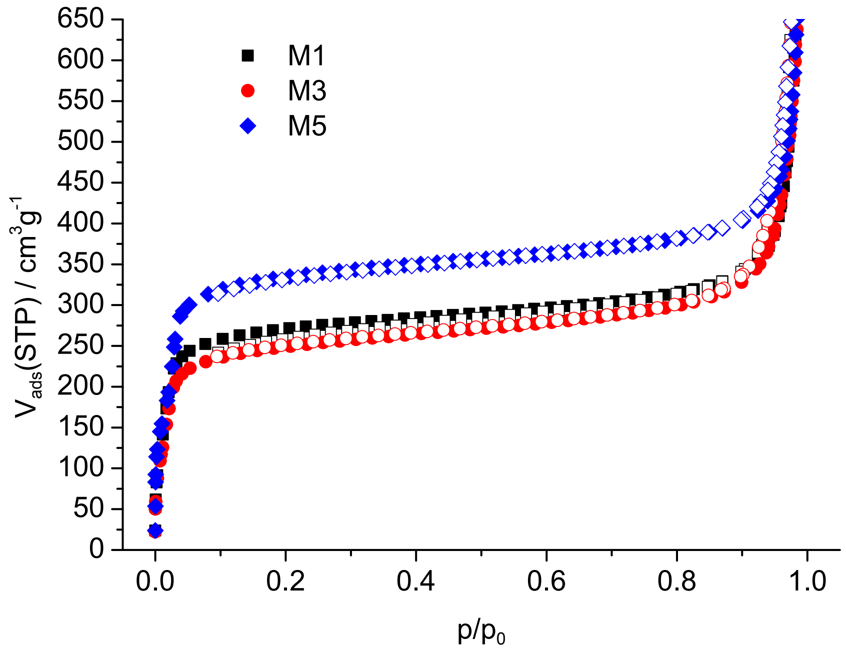

Fig. S45. Results of N$_2$ sorption measurements of the activated (70 °C, 10^{-2} kPa) Ce/Zr-MOF-808 compounds M1, M3 and M5. Filled symbols mark the adsorption, while empty symbols mark the desorption step. All compounds exhibit Type I(a) adsorption isotherms with small additional steps at $p/p_0 = 0.025$ due to the filling of pores of different sizes.

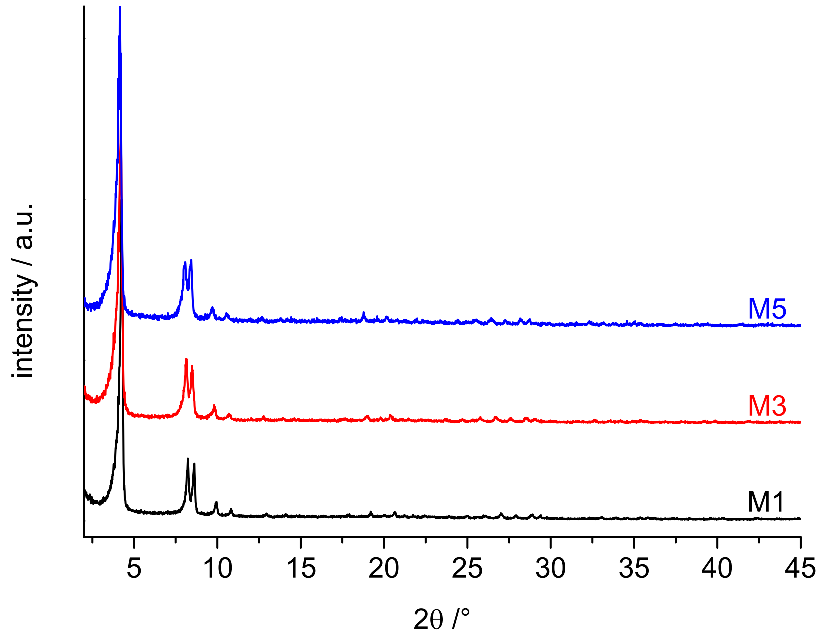

Fig. S46. PXRD patterns (λ= 1.5406 Å) of the bimetallic Ce/Zr-MOF-808 compounds after the N_2 sorption measurement.

---

1 M. Thommes, K. Kaneko, A. V. Neimark, J. P. Olivier, F. Rodriguez-Reinoso, J. Rouquerol and S. W. Sing Kenneth, *Pure Appl. Chem.*, 2015, **87**, 1051-1069.

2 M. Lammert, M. T. Wharmby, S. Smolders, B. Bueken, A. Lieb, K. A. Lomachenko, D. D. Vos and N. Stock, *Chem. Commun.*, 2015, **51**, 12578-12581.

3 J. H. Cavka, S. Jakobsen, U. Olsbye, N. Guillou, C. Lamberti, S. Bordiga and K. P. Lillerud, *J. Am. Chem. Soc.*, 2008, **130**, 13850-13851.

4 F. Nouar, M. I. Breeze, B. C. Campo, A. Vimont, G. Clet, M. Daturi, T. Devic, R. I. Walton and C. Serre, *Chem. Commun.*, 2015, **51**, 14458-14461.

5 H. Furukawa, F. Gándara, Y.-B. Zhang, J. Jiang, W. L. Queen, M. R. Hudson and O. M. Yaghi, *J. Am. Chem. Soc.*, 2014, **136**, 4369-4381.

6 M. Lammert, C. Glißmann, H. Reinsch and N. Stock, *Cryst. Growth Des.*, 2016, DOI: 10.1021/acs.cgd.1026b01512.